A Target-Based Self-Calibration Method for Terrestrial Laser Scanners and its Robust Solution

Peng Lin, Xiaojun Cheng, Tengfei Zhou, Chao Liu, and Bin Wang

***Abstract*—Fundamental systematic errors in point cloud data are inevitable due to a variety of factors, ranging from the external environment during scanning or observation by a terrestrial laser scanner (TLS) to the assembly of the instrument. For low-cost scanners, error terms may be further accentuated and included, in addition to systematic errors, random or even serious errors that directly affect the coordinates of each point in the point cloud, which are directly related to the quality of the point cloud data and subsequent processing. To address the above issues, we attempted to propose a robust target-based self-calibration method for TLS at the algorithmic level without considering the network design and measurement configuration, and derived its solution by normalizing the residual vector and calculating an equivalent covariance matrix based on the IGG III function. After validating the simulated and measured data, the experimental results showed that the proposed self-calibration method could effectively eliminate the random and gross errors associated with the observations; improved the accuracy of the points from centimeter to millimeter level; and increased the accuracy of the corrected checkpoints by 58%, 47%, and 33%, respectively, compared to the three existing methods. However, the proposed method was unable to take into account the attenuation of parameter correlations and further refinement in terms of measurement configurations would be subsequently required.**

***Index Terms*—Calibration, laser measurements, measurement errors, nonlinear estimation, robustness.**

I. Introduction

As an up-and-coming measurement technology, terrestrial laser scanner (TLS) has the benefits of being fast, noncontact, and proactive; the point cloud data it obtains allows for the inclusion of geometric and physical information about the targets, and provides high density and accuracy [1]. Inevitably, during the scanning or observation of an object, the quality of the point cloud is susceptible to various factors, e.g., the target itself and the external environment, as well as the instrument itself [2]–[5], which make the point cloud data often contains a part of systematic errors or even gross errors in addition to the random ones, resulting in the output results are challenging to reflect the real properties of the targets, reducing the observation accuracy and affecting the subsequent point cloud processing to a certain extent.

Consequently, a method is basically required, if possible, to correctly and effectively eliminate the various errors in observations, which is also called instrument calibration. Instrument calibration in the general sense is only for systematic errors and does not take into account random and gross errors. In order to achieve this, traditional methods usually divide the observations into two categories, namely distances and angles [6], [7]. The overall objective is that the effect of the remaining systematic errors (i.e., deviations) after calibration should be sufficiently small or, in other words, insignificant. The specific implementation process involves measuring a baseline or fixed angle of defined length using the instrument to be calibrated followed by an indirect adjustment or other algorithm to solve for the relevant calibration parameters (CPs). This demonstrates that conventional methods require a relatively rigorous experimental environment and high accuracy baselines and angles, with all of these having to be maintained on a regular basis. In contrast, self-calibration methods avoid such necessities. After the observations are obtained, the CPs would be treated as unknown parameters and briefly introduced into some functional model to determine [8].

Generally, self-calibration methods can be divided into point-based and surface-based according to different fundamentals. For the first type, Lichti [9], [10] made a comprehensive analysis of the CPs in the distance and angle of TLS observations, proposed a point-based TLS self-calibration model based on the rigid body transformation model, and realized the estimation of CPs for FARO880. González *et al.* [11] investigated eight systematic errors in the original observations, which belong to laser rangefinder, beam deflection unit, and rotation platform, then constructed a function model based on rigid body transformation model, with stochastic model applying nominal accuracy and covariance propagation law, to complete the calibration of Trimble GX200 and Riegl LMS–Z390i. Holst [12] introduced the concept of calibration where only one object and one scan were employed, using the deviation of each sampling point from the scanned object to calibrate the instrument. Lerma [13] suggested a method for determining the optimal set of additional parameters, which provided the best mathematical

Manuscript received April 29, 2021; revised August 16, 2021; accepted November 5, 2021. Date of publication November 9, 2021; date of current version December 6, 2021. This work was supported in part by the Youth project of Anhui Natural Science Foundation under Grant 2008085QD179, in part by the National Natural Science Foundation of China under Grant 41974213, and in part by the Science and Technology Project of Hebei Education Department under Grant ZD2021023. *(Corresponding author: Tengfei Zhou.)*

Peng Lin is with the College of Civil Engineering, Anhui Jianzhu University, Hefei 230000, China (e-mail: penglin1991@ahjzu.edu.cn).

Xiaojun Cheng and Tengfei Zhou are with the College of Survey and Geo-Informatics, Tongji University, Shanghai 200092, China (e-mail: cxj@tongji.edu.cn; 1710639@tongji.edu.cn).

Chao Liu is with the School of Mining and Geomatics, Hebei University of Engineering, Handan 056038, China (e-mail: chaoliu0202@gmail.com).

Bin Wang is with the School of Geomatics Science and Technology, Nanjing Tech University, Nanjing 211816, China (e-mail: binwangsgg@njtech.edu.cn).

Digital Object Identifier 10.1109/JSTARS.2021.3126452

solution on the basis of the dimensionless mass index. Reshetyuk [14] implemented the Callidus 1.1, HDS3000, and HDS2500 in an indoor three-dimensional (3-D) calibration field, referring to [15], [16] for more details. Li *et al.* [17] achieved TLS self-calibration through a background target-based approach by extracting feature points via a key point quality algorithm without the use of auxiliary targets and prior knowledge. Guan *et al.* [4] implemented the self-calibration of the HDS3000 using rigid body transformation and nonlinear least squares, with reference to the total station (TS) measurement system for the selection of the system errors. Medić *et al.* [18] introduced 10 CPs into the observations and performed the *in-situ* calibration during the measurements to study the stability of the CPs. Zhou *et al.* [2] implemented the estimation of the systematic error of Leica HDS3000 based on the adoption of CPs in [9], and solved the problem of weighting different classes of observations using the variance component estimation (VCE) theory. Li *et al.* [19] estimated five types of angular errors for the Lab-built TLS by the two-sided method and the network method.

In addition, the correlation among the estimated parameters needs to be addressed in order to improve the estimation accuracy of the CPs [20]–[24]. Medić *et al.* [25] investigated point-based self-calibrating empirical stochastic models that address the problem of conventional stochastic models that do not match the facts by studied the accuracy of target centroid detection. In the self-calibration process, in addition to ensuring the stability and effective distribution of the feature points, the configuration and the number of stations are still related to the final results [24], [26]–[28]. Besides, plane-based methods are also very commonly used [17], [27], [29]–[31]. If there are problems with the experimental design and implementation process, perhaps the solution can be found in [32], [33].

A comprehensive analysis of self-calibration literature in recent years shows that most of the methods are implemented via the rigid coordinate transformation model, ignoring the random errors of the original observations, and do not consider whether these methods can be well resolved when there are gross errors in coordinate sequences which could lead to the function model to be incorrect, although it is possible to obtain adjusted results.

To address these considerations, we have developed an approach for TLS self-calibration on the basis of the Gauss–Helmert model and the TLS observation principle, subject to the introduction of random errors for all observations; on the other hand, for the stochastic model, observations were weighted with nominal accuracy deemed to be *a priori* information and the gross values are posteriori weighted by applying the IGG III function with standardized residuals. In addition, in order to enable weighting of several categories of observations (distances and angles), given that the *a priori* unit-weighted medium errors of distance and angle should not be theoretically the same [34]–[36], the VCE was introduced for the posterior estimation of the observations. In this article, only the model itself and the algorithm were studied, and aspects such as the configuration of the measurement and the targets distribution were not analyzed yet.

The rest of this article is organized as follows: Section II mainly introduces the observation principle of TLS and theory of self-calibration based on coordinate transformation model. Section III describes our proposed model and derives its robust solution. The experiments and discussions are presented in Section IV. Finally, we conclude the article with a summary of our work and future research considerations in Section V.

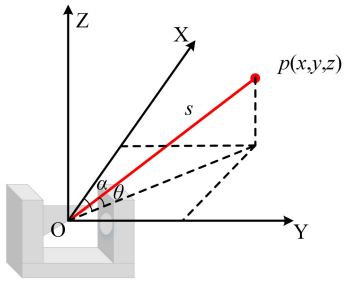

Fig. 1. Observations of TLS. *X*-axis represents the collimation axis; *Y*-axis is the horizontal axis; and *Z*-axis is the vertical axis.

II. Theory of Self-Calibration

The TLS enables rapid scanning and measurement of target objects through the organic combination of a laser rangefinder and an angular measuring system. During this period, the 3-D coordinates of the point cloud are defined in the left-hand coordinate system determined by the TLS, with the *XOY* plane as the transverse scanning plane and the *Z*-axis perpendicular to the *XOY* plane [20], [37].

In Fig. 1, p denotes the target point; (x, y, z) are the Cartesian coordinate of p. (s, θ, α) represents the original observations in the spherical coordinate system, i.e., original observations, with the means of oblique distance, vertical angle, and horizontal angle sequentially.

For the geometric information described above, the TLS in field of view (FOV), whether pulsed or phased, proceeds by measuring the distance from the scanning point to the geometric center of the instrument by means of the photoelectric distance measuring principle, which, in combination with the angular observations obtained with the angle encoder, records the polar coordinates of the target object. Depending on the interrelationships between the coordinate systems, the original observations can be converted into spatial Cartesian coordinates via:

$$\begin{cases} x = s \cdot cos\theta \cdot cos\alpha \\ y = s \cdot cos\theta \cdot sin\alpha \\ z = s \cdot sin\theta. \end{cases} \tag{1}$$

Here, (1) is considered to be the observation equation of TLS. Similarly, original observation can also be derived from Cartesian coordinates if needed:

$$\begin{cases} s = \sqrt{x^2 + y^2 + z^2} \\ \theta = \tan^{-1}\left(z/\sqrt{x^2 + y^2}\right) \\ \alpha = \tan^{-1}(y/x). \end{cases} \tag{2}$$

As is well recognized, there must be a degree of deviation in the relative spatial position of the elements between the actual and ideal states during the machining and manufacture of the instrument, although these differences may be small.

Consequently, the initial observed values would not always correspond to the optimum values, but contain both random and systematic errors. In the case of systematic errors, introducing the elements in [10], [27], distances are generally involved with the addition constant m, multiplication constant λ; the angles accommodate the collimation axis error c, vertical axis error i, and horizontal axis error t. These five unknowns are treated as CPs in a common sense, and it should be noted that the effect of c and i on horizontal angle observations is related to that of vertical angle observations:

$$c' = c/\cos\theta, i' = i \cdot \tan\theta. \tag{3}$$

As a matter of practice, for target-based self-calibration methods, simultaneous or sequential measurements of common points by a TS with high accuracy and a scanner to be calibrated are commonly undertaken. It is required that these points are evenly distributed in space to ensure validity and also to avoid possible pathologies in the calculation process. Afterwards, the coordinates obtained by the two instruments can be manipulated to calculate the CPs by means of a rigid body transformation model based on the least squares method:

$$\begin{aligned}\begin{bmatrix} X \\ Y \\ Z \end{bmatrix} &= \mathbf{R}\begin{bmatrix} x \\ y \\ z \end{bmatrix} + \begin{bmatrix} \Delta x \\ \Delta y \\ \Delta z \end{bmatrix} \\ &= \mathbf{R}\begin{bmatrix} [s\cdot(1+\lambda)+m]\cdot cos(\theta+t)\cdot cos(\alpha+c'+i') \\ [s\cdot(1+\lambda)+m]\cdot cos(\theta+t)\cdot sin(\alpha+c'+i') \\ [s\cdot(1+\lambda)+m]\cdot sin(\theta+t) \end{bmatrix} \\ &\quad + \begin{bmatrix} \Delta x \\ \Delta y \\ \Delta z \end{bmatrix}\end{aligned} \tag{4}$$

where $[X, Y, Z]^{\mathrm{T}}$is the vector of Cartesian coordinate under TS system; $[\Delta x, \Delta y, \Delta z]^{\mathrm{T}}$ represents translation parameters; and $\boldsymbol{R}$ is represented as a rotation matrix consisting of three rotation parameters, which can be conducted by multiplying three matrices as follows:

$$\mathbf{R} = \mathbf{R}_{\varphi}\mathbf{R}_{\omega}\mathbf{R}_{\kappa} \tag{5}$$

where

$$\mathbf{R}_{\varphi} = \begin{bmatrix} \cos\varphi & 0 & -\sin\varphi \\ 0 & 1 & 0 \\ \sin\varphi & 0 & \cos\varphi \end{bmatrix} \tag{6}$$

$$\mathbf{R}_{\omega} = \begin{bmatrix} 1 & 0 & 0 \\ 0 & \cos\omega & -\sin\omega \\ 0 & \sin\omega & \cos\omega \end{bmatrix} \tag{7}$$

$$\mathbf{R}_{\kappa} = \begin{bmatrix} \cos\kappa & -\sin\kappa & 0 \\ \sin\kappa & \cos\kappa & 0 \\ 0 & 0 & 1 \end{bmatrix}. \tag{8}$$

Here, $(\varphi, \omega, \kappa)$ represents the Euler angles between the corresponding axis of the two coordinate systems. Although $\boldsymbol{R}$ has multiple manifestations, but the results are the same, only the order of rotation differs. For greater clarity, we referred to $(\Delta x, \Delta y, \Delta z, \varphi, \omega, \kappa)$ as EOPs in our proposed algorithm.

III. Self-Calibration Method for Low-Cost Scanners

The self-calibration function model described above, i.e., (4), reveals that only CPs and EOPs are treated as unknowns to be estimated in the calculation of the parameters. In response to the above analysis and discussion, and to effectively accommodate random and gross errors along with different types of observations, a novel self-calibrating function model was developed for TLS based on the Gauss–Helmert model. This article is dedicated to achieve the following objectives:

1) Using the weighted total least squares (WTLS) algorithm to realize the derivation and linearization of the proposed model.
2) Constructing a stochastic model with a similar form to [21] to address the deterioration of the random errors on parameters' solution.
3) Reweighting the observations containing gross errors via normalized residuals with IGG III weight factor function to achieve robust performance of the method.
4) Employing VCE method and further weighting the observations according to the residuals, which is due to the fact that distance and angle are of different classes.

A. Self-Calibration Model

Since the observations obtained by TS and TLS are 3-D spatial right-angle coordinates, in order to rationalize the introduction of VCE reasonably, the TS observations need to be replaced by the original observations either, i.e., distances and angles, apart from the observations of TLS. Furthermore, accounting for random errors in all original values, the self-calibration function model can be written as follows:

$$\begin{aligned}&\begin{bmatrix} (\rho-e_{\rho})\cos(\gamma-e_{\gamma})\cos(\beta-e_{\beta}) \\ (\rho-e_{\rho})\cos(\gamma-e_{\gamma})\sin(\beta-e_{\beta}) \\ (\rho-e_{\rho})\sin(\gamma-e_{\gamma}) \end{bmatrix}_{\mathrm{TS}} = \\ &\mathbf{R}\begin{bmatrix} [(s-e_s)(1+\lambda)+m]\cos(\theta-e_{\theta}+t)\cos(\alpha-e_{\alpha}+i'+c') \\ [(s-e_s)(1+\lambda)+m]\cos(\theta-e_{\theta}+t)\sin(\alpha-e_{\alpha}+i'+c') \\ [(s-e_s)(1+\lambda)+m]\sin(\theta-e_{\theta}+t) \end{bmatrix}_{\mathrm{TLS}} \\ &+ \begin{bmatrix} \Delta X \\ \Delta Y \\ \Delta Z \end{bmatrix}\end{aligned} \tag{9}$$

where the subscripts on the outside of the matrices indicate their coordinate system. (ρ, γ, β) and (s, θ, α) denote the original observations under the coordinate systems of TS and TLS, respectively. The variables with e are the random errors corresponding to the various types of observations, and can be substituted as

$$\begin{cases} \mathbf{e}_{\mathrm{TS}} = [\, e_{\rho}\ e_{\gamma}\ e_{\beta}\,]^T \\ \mathbf{e}_{\mathrm{TLS}} = [\, e_s\ e_{\theta}\ e_{\alpha}\,]^T \end{cases} \tag{10}$$

where $(e_s, e_{\theta}, e_{\alpha})$ and $(e_{\rho}, e_{\gamma}, e_{\beta})$ are the random errors of the distance and angle observations in the TS and TLS systems, respectively; and $\mathbf{e}_{\mathrm{TS}}$ and $\mathbf{e}_{\mathrm{TLS}}$ are their overall representations.

According to the above function model, namely (9), it is not difficult to find that, unlike the TLS observations, the coordinates in TS do not include the systematic parameters, which is because

in the scanner self-calibration process, in order to obtain high precision systematic errors or the so-called self–CPs, higher precision TS is typically adopted to observe the same series of targets as the scanner. On the other hand, random errors in the observations are unavoidable, so the random errors in the original observations of both systems are not neglected, and they are considered as variables obeying normal distribution [38], [39]. With a reference to nominal accuracy σ, the stochastic models under TS and TLS system can be expressed with the following notations:

$$\mathbf{e}_{\mathrm{TLS}} = \begin{bmatrix} e_s \\ e_\theta \\ e_\alpha \end{bmatrix} \sim \left(\begin{bmatrix} 0 \\ 0 \\ 0 \end{bmatrix}, \begin{bmatrix} \sigma_s^2 & 0 & 0 \\ 0 & \sigma_\theta^2 & 0 \\ 0 & 0 & \sigma_\alpha^2 \end{bmatrix} \right) \tag{11}$$

$$\mathbf{e}_{\mathrm{TS}} = \begin{bmatrix} e_\rho \\ e_\gamma \\ e_\beta \end{bmatrix} \sim \left(\begin{bmatrix} 0 \\ 0 \\ 0 \end{bmatrix}, \begin{bmatrix} \sigma_\rho^2 & 0 & 0 \\ 0 & \sigma_\gamma^2 & 0 \\ 0 & 0 & \sigma_\beta^2 \end{bmatrix} \right). \tag{12}$$

B. Derivation of the Proposed Method

In the function model, (9), the independent and dependent variables are linked by a nonlinear mathematical expression, and therefore the proposed method is not a linear model, essentially a variant of the Gauss–Helmert model [40]. A regularly practiced approach is to convert a nonlinear regression into a linear regression by means of variable transformation [40], [41]. The specific process is to linearize the function model employing the Gauss–Newton method, then construct the Lagrange objective function for the expanded function model and derive solutions for the parameters based on their necessary conditions, i.e., the function has zero partial derivatives with respect to each variable.

We assumed that the initial values of the random errors in the TS and TLS coordinate systems are as follows:

$$\mathbf{e}_{\mathrm{TLS}}^0 = [\, e_s^0 \; e_\theta^0 \; e_\alpha^0 \,]^{\mathrm{T}}, \mathbf{e}_{\mathrm{TS}}^0 = [\, e_\rho^0 \; e_\gamma^0 \; e_\beta^0 \,]^{\mathrm{T}}. \tag{13}$$

For better distinguishing, only the superscripts of 0 represent the initial values, while the superscript j in the following indicates the index of iterations. The corresponding unknown parameters in the function model, including EOPs and CPs, are set to

$$\xi^0 = \left[\, \Delta x^0 \; \Delta y^0 \; \Delta z^0 \; \varphi^0 \; \omega^0 \; \kappa^0 \; m^0 \; \lambda^0 \; c^0 \; i^0 \; t^0 \,\right]^T. \tag{14}$$

Since the initial values do not need to be very precise, for the EOPs in the unknown parameters, the conventional linear Gauss–Markov model, or even the Bursa–Wolf model (which needs to ignore the effect of scale scaling), was validated to be available [40]–[42]. It was hypothesized that all instruments were in ideal condition when assembled and measured in the field, and therefore the initial values of CPs in the parameter vector and the random error vector corresponding to the original observation could be approximated as zero.

For ease of reading and understanding, some alphabetic variables were appointed to represent the matrices in the derivation to achieve simplification of the function model. We substituted the symbol $\boldsymbol{H}$ for the observation equation with random errors in the two datum, the symbol $\boldsymbol{T}$ for the translation parameters vector. The subscripts 1 and 2 in following equations stand for TS and TLS, respectively. The right end of (9) is expanded at the set approximation ξ^0according to the binary Taylor series. After retaining the terms of first order, the linearized function model can be conducted as

$$\begin{aligned} &\mathbf{H}_1^j + \mathbf{A}_1^j \left(\mathbf{e}_1 - \mathbf{e}_1^j \right) \\ &\quad = \mathbf{R}^j \mathbf{H}_2^j + \mathbf{T}^j + d\mathbf{T} \\ &\qquad + \frac{\partial \mathbf{R}^j}{\partial \varphi} \mathbf{H}_2^j d\varphi + \frac{\partial \mathbf{R}^j}{\partial \omega} \mathbf{H}_2^j d\omega + \frac{\partial \mathbf{R}^j}{\partial \kappa} \mathbf{H}_2^j d\kappa \\ &\qquad + \mathbf{R}^j \frac{\partial \mathbf{H}_2^j}{\partial m} dm + \mathbf{R}^j \frac{\partial \mathbf{H}_2^j}{\partial \lambda} d\lambda + \mathbf{R}^j \frac{\partial \mathbf{H}_2^j}{\partial c} dc + \mathbf{R}^j \frac{\partial \mathbf{H}_2^j}{\partial i} di \\ &\qquad + \mathbf{R}^j \frac{\partial \mathbf{H}_2^j}{\partial t} dt + \mathbf{R}^j \frac{\partial \mathbf{H}_2^j}{\partial \mathbf{e}_2} \left(\mathbf{e}_2 - \mathbf{e}_2^j \right). \end{aligned} \tag{15}$$

The model after linearization based on Gauss–Newton method must be iterated continuously when calculating the unknowns until termination conditions are met [41], which means that when $j = 1$, i.e., the first iteration, the variables involved in function model need to be populated with the initial values, and during the subsequent iterations of the calculation, these variables need to be replaced with the results computed last time; ∂ is the partial derivation symbol.

As the course of performing partial derivatives involves a large number of variables, and even some of them recur from time to time. The arithmetic operations of some variables can be represented by the new notation, primarily corrections of original observations, for sake of obtaining a concise form of the linear expression. We substituted

$$\begin{cases} s^j = \left(s - e_s^j \right) \left(1 + \lambda^j \right) + m, \theta^j = \theta - e_\theta^j + t^j \\ \alpha^j = \alpha - e_\alpha^j + (c')^j + (i')^j \\ \chi^j = c \sec \theta^j \tan \alpha^j + i \sec^2 \theta^j \\ \rho^j = \rho - e_\rho^j, \gamma^j = \gamma - e_\gamma^j, \beta^j = \beta - e_\beta^j. \end{cases} \tag{16}$$

Correspondingly, the partial derivatives of the observation equation concerning the random errors, i.e., $\mathbf{A}_1^j$and $\mathbf{A}_2^j$, as well as the coefficient matrix of each CPs can be conducted as follows:

$$\begin{cases} \frac{\partial \mathbf{H}_2^j}{\partial m} = \begin{bmatrix} \cos\theta^j \cos\alpha^j \\ \cos\theta^j \sin\alpha^j \\ \sin\theta^j \end{bmatrix} \\ \frac{\partial \mathbf{H}_2^j}{\partial \lambda} = \left(s - e_s^j \right) \begin{bmatrix} \cos\theta^j \cos\alpha^j \\ \cos\theta^j \sin\alpha^j \\ \sin\theta^j \end{bmatrix} \\ \frac{\partial \mathbf{H}_2^j}{\partial c} = \frac{1}{\cos\theta^j} \begin{bmatrix} -s^j \cos\theta^j \sin\alpha^j \\ s^j \cos\theta^j \cos\alpha^j \\ 0 \end{bmatrix} \\ \frac{\partial \mathbf{H}_2^j}{\partial i} = \tan\theta^j \begin{bmatrix} -s^j \cos\theta^j \sin\alpha^j \\ s^j \cos\theta^j \cos\alpha^j \\ 0 \end{bmatrix} \\ \frac{\partial \mathbf{H}_2^j}{\partial t} = \begin{bmatrix} s^j(-\sin\theta^j \cos\alpha^j - \chi^j \cos\theta^j \sin\alpha^j) \\ s^j(-\sin\theta^j \sin\alpha^j + \chi^j \cos\theta^j \cos\alpha^j) \\ s^j \cos\theta^j \end{bmatrix} \end{cases} \tag{17}$$

Combining (15)–(19), (18) and (19) shown at the bottom of this page, and merging the similar terms results in the simplified functional model as follows:

$$\mathbf{H}_1^j + \mathbf{A}_1^j\left(\mathbf{e}_1 - \mathbf{e}_1^j\right) = \mathbf{R}^j\mathbf{H}_2^j + \mathbf{T}^j + \mathbf{B}^j d\xi^{j+1} + \mathbf{A}_2^j\left(\mathbf{e}_2 - \mathbf{e}_2^j\right). \tag{20}$$

Here, $\boldsymbol{B}$ represents the coefficient matrix of the new parameters vector $d\hat{\xi}$, due to the unknown parameters to be solved will be changed into the corrected values of the original parameters at this point. $\boldsymbol{B}$ and $d\hat{\xi}$ are characterized by the following expressions:

$$d\hat{\xi} = \left[d\Delta x\ d\Delta y\ d\Delta z\ d\varphi\ d\omega\ d\kappa\ dm\ d\lambda\ dc\ di\ dt\right]^T \tag{21}$$

$$\mathbf{B}^j = \begin{bmatrix} \mathbf{E}_{3\times3}\ \frac{\partial\mathbf{R}^j}{\partial\varphi}\mathbf{H}_2^j\ \frac{\partial\mathbf{R}^j}{\partial\omega}\mathbf{H}_2^j\ \frac{\partial\mathbf{R}^j}{\partial\kappa}\mathbf{H}_2^j\ \mathbf{R}^j\frac{\partial\mathbf{H}_2^j}{\partial m}\ \mathbf{R}^j\frac{\partial\mathbf{H}_2^j}{\partial\lambda} \\ \mathbf{R}^j\frac{\partial\mathbf{H}_2^j}{\partial c}\ \mathbf{R}^j\frac{\partial\mathbf{H}_2^j}{\partial i}\ \mathbf{R}^j\frac{\partial\mathbf{H}_2^j}{\partial t} \end{bmatrix}. \tag{22}$$

Here, $\mathbf{E}_{3\times3}$ is a unit matrix of dimension three.

Under the condition of considering the stochastic information of the observations, the stochastic model inaccessibly needs to be constructed to reflect the effect of each observation on the parameters' estimation:

$$\mathbf{e} = \begin{bmatrix}\mathbf{e}_1\\ \mathbf{e}_2\end{bmatrix} \sim \left(\begin{bmatrix}0\\0\end{bmatrix}, \sigma_0^2\begin{bmatrix}\mathbf{Q}_1\\ \mathbf{Q}_2\end{bmatrix}\right). \tag{23}$$

σ_0 is the *a priori* medium error; $\mathbf{Q}_1$ and $\mathbf{Q}_2$ are the observed value cofactor matrices of TS and TLS systems, respectively.

By using the estimation criterion of least squares as compliance, the objective of the proposed method can be written as

$$\mathbf{V}^{\mathrm{T}}\mathbf{P}\mathbf{V} = \min \tag{24}$$

where

$$\begin{cases}\mathbf{V} = \begin{bmatrix}\mathbf{e}_1\ \mathbf{e}_2\end{bmatrix}^{\mathrm{T}} \\ \mathbf{P} = \begin{bmatrix}\mathbf{P}_1 & \\ & \mathbf{P}_2\end{bmatrix} = \begin{bmatrix}\mathbf{Q}_1^{-1} & \\ & \mathbf{Q}_2^{-1}\end{bmatrix} = \mathbf{Q}^{-1}.\end{cases} \tag{25}$$

Here, $\boldsymbol{P}$ is the weight matrix of observations; and $\boldsymbol{Q}$ represents the covariance matrix and is reciprocal to the $\boldsymbol{P}$ matrix.

Through the above linearized functional model, (20), based on the Gauss–Newton iterative method and taking into account the premise of the new estimation criterion, the solution of parameters can be natively deduced by Lagrange objective function:

$$\Phi = \mathbf{e}_1^{\mathrm{T}}\mathbf{P}_1\mathbf{e}_1 + \mathbf{e}_2^{\mathrm{T}}\mathbf{P}_2\mathbf{e}_2 + 2\mathbf{K}^{\mathrm{T}}\left(\mathbf{L}^j - \mathbf{B}^j d\hat{\xi}^j + \mathbf{A}_1^j\mathbf{e}_1 - \mathbf{A}_2^j\mathbf{e}_2\right) \tag{26}$$

where

$$\mathbf{L}^j = \mathbf{H}_1^j - \mathbf{A}_1^j\mathbf{e}_1^j - \mathbf{R}^j\mathbf{H}_2^j - \mathbf{T}^j + \mathbf{A}_2^j\mathbf{e}_2^j. \tag{27}$$

$\boldsymbol{K}$ is the Lagrange multiplier; the weight matrices $\mathbf{P}_1$ and $\mathbf{P}_2$ of the two coordinate systems are block diagonal matrices whose elements need to be arranged in the same order as the ranking of the residual vector $\boldsymbol{e}$:

$$\begin{cases}\mathbf{P}_1 = \mathrm{blkdiag}\left(\frac{\sigma_0^2}{\sigma_\rho^2}\ \frac{\sigma_0^2}{\sigma_\gamma^2}\ \frac{\sigma_0^2}{\sigma_\beta^2}\right) \\ \mathbf{P}_2 = \mathrm{blkdiag}\left(\frac{\sigma_0^2}{\sigma_s^2}\ \frac{\sigma_0^2}{\sigma_\theta^2}\ \frac{\sigma_0^2}{\sigma_\alpha^2}\right)\end{cases} \tag{28}$$

where "blkdiag" denotes the block diagonal matrix; the *a priori* unit weight medium error is located in the numerator position, and the symbols in the denominator position indicate the *a priori* information of the original observation, which can be generally obtained through the nominal accuracy given by the instrument manufacturer.

The corrections to the unknown parameters and the estimates of the residuals of the observations can be readily obtained, according to the Lagrange necessary condition that the partial derivatives of the objective function with respect to each variable

$$\begin{cases}\frac{\partial\mathbf{R}^j}{\partial\varphi} = \frac{\partial\mathbf{R}_\varphi^j}{\partial\varphi}\mathbf{R}_\omega^j\mathbf{R}_\kappa^j = \begin{bmatrix}-\mathbf{R}^j(3,1) & -\mathbf{R}^j(3,2) & -\mathbf{R}^j(3,3)\\ 0 & 0 & 0\\ \mathbf{R}^j(1,1) & \mathbf{R}^j(1,2) & \mathbf{R}^j(1,3)\end{bmatrix} \\ \frac{\partial\mathbf{R}^j}{\partial\omega} = \mathbf{R}_\varphi^j\frac{\partial\mathbf{R}_\omega^j}{\partial\omega}\mathbf{R}_\kappa^j = \begin{bmatrix}-\sin\varphi^j\mathbf{R}^j(2,1) & -\sin\varphi^j\mathbf{R}^j(2,2) & -\sin\varphi^j\mathbf{R}^j(2,3)\\ -\sin\omega^j\sin\kappa^j & -\sin\omega^j\cos\kappa^j & -\cos\omega^j\\ \cos\varphi^j\mathbf{R}^j(2,1) & \cos\varphi^j\mathbf{R}^j(2,2) & \cos\varphi^j\mathbf{R}^j(2,3)\end{bmatrix} \\ \frac{\partial\mathbf{R}^j}{\partial\kappa} = \mathbf{R}_\varphi^j\mathbf{R}_\omega^j\frac{\partial\mathbf{R}_\kappa^j}{\partial\kappa} = \begin{bmatrix}\mathbf{R}^j(1,2) & -\mathbf{R}^j(1,1) & 0\\ \mathbf{R}^j(2,2) & -\mathbf{R}^j(2,1) & 0\\ \mathbf{R}^j(3,2) & -\mathbf{R}^j(3,1) & 0\end{bmatrix}\end{cases} \tag{18}$$

$$\begin{cases}\mathbf{A}_1^j = \frac{\partial\mathbf{H}_1}{\partial\mathbf{e}_1} = \begin{bmatrix}-\cos\gamma^j\cos\beta^j & \rho^j\sin\gamma^j\cos\beta^j & \rho^j\cos\gamma^j\sin\beta^j\\ -\cos\gamma^j\sin\beta^j & \rho^j\sin\gamma^j\sin\beta^j & -\rho^j\cos\gamma^j\cos\beta^j\\ -\sin\gamma^j & -\rho^0\cos\gamma^0 & 0\end{bmatrix} \\ \mathbf{A}_2^j = \mathbf{R}^j\frac{\partial\mathbf{H}_2}{\partial\mathbf{e}_2} = \mathbf{R}^j\begin{bmatrix}-(1+\lambda^j)\cos\theta^j\cos\alpha^j & s^j(\sin\theta^j\cos\alpha^j + \chi^j\cos\theta^j\sin\alpha^j) & s^j\cos\theta^j\sin\alpha^j\\ -(1+\lambda^j)\cos\theta^j\sin\alpha^j & s^j(\sin\theta^j\sin\alpha^j - \chi^j\cos\theta^j\cos\alpha^j) & -s^j\cos\theta^j\cos\alpha^j\\ -(1+\lambda^j)\sin\theta^j & -s^j\cos\theta^j & 0\end{bmatrix}\end{cases} \tag{19}$$

(a) (b)

Fig. 2. Results of centroid extraction. (a) Rational result. (b) Result with gross errors.

are zero:

$$\begin{cases} \frac{1}{2}\frac{\partial \Phi}{\partial \mathbf{e}_1} = \mathbf{P}_1\tilde{\mathbf{e}}_1 + \left(\mathbf{A}_1^j\right)\hat{\mathbf{K}} = 0 \\ \frac{1}{2}\frac{\partial \Phi}{\partial \mathbf{e}_2} = \mathbf{P}_2\tilde{\mathbf{e}}_2 - \left(\mathbf{A}_2^j\right)\hat{\mathbf{K}} = 0 \\ \frac{1}{2}\frac{\partial \Phi}{\partial \mathrm{d}\hat{\xi}} = -\left(\mathbf{B}^j\right)^{\mathrm{T}}\hat{\mathbf{K}} = 0 \\ \frac{1}{2}\frac{\partial \Phi}{\partial \hat{\mathbf{K}}} = \mathbf{L}^j - \mathbf{B}^j\mathrm{d}\hat{\xi}^j + \mathbf{A}_1^j\tilde{\mathbf{e}}_1 - \mathbf{A}_2^j\tilde{\mathbf{e}}_2 = 0 \end{cases} \tag{29}$$

where

"^" represents the estimated values; and "∼" denotes the predicted values.

After processing (29), the following results can be readily derived:

$$\mathrm{d}\hat{\xi}^j = \left(\left(\mathbf{B}^j\right)^{\mathrm{T}}\left(\mathbf{Q}_c^j\right)^{-1}\mathbf{B}^j\right)^{-1}\left(\mathbf{B}^j\right)^{\mathrm{T}}\left(\mathbf{Q}_c^j\right)^{-1}\mathbf{L}^j \tag{30}$$

$$\begin{bmatrix}\tilde{\mathbf{e}}_1 \\ \tilde{\mathbf{e}}_2\end{bmatrix} = \begin{bmatrix} -\mathbf{Q}_1\left(\mathbf{A}_1^j\right)^{\mathrm{T}}\left(\mathbf{Q}_c^j\right)^{-1} \\ \mathbf{Q}_2\left(\mathbf{A}_2^j\right)^{\mathrm{T}}\left(\mathbf{Q}_c^j\right)^{-1}\end{bmatrix}\left(\mathbf{L}^j - \mathbf{B}^j\mathrm{d}\hat{\xi}^j\right) \tag{31}$$

where

$$\mathbf{Q}_c^j = \mathbf{A}_1^j\mathbf{Q}_1\left(\mathbf{A}_1^j\right)^{\mathrm{T}} + \mathbf{A}_2^j\mathbf{Q}_2\left(\mathbf{A}_2^j\right)^{\mathrm{T}}. \tag{32}$$

Although following the above process, it is possible to derive the scanner self-CPs in the case of considering random errors; however, the method has no resistance to gross errors when they are present in the observed data because of the lack of *a posteriori* estimation of the weight matrix [43].

C. Robust Estimation

In the procedures such as scanning and feature point extraction, it is often difficult to capture the center point of a target with high accuracy, especially when a low-cost scanner is deployed. In some cases, the extracted coordinates also deviate from the centroid to a large extent, resulting in coordinates containing gross errors, which are critical for instrument calibration, since least squares-based methods are not resistant to gross deviations, which can have a significant impact on the final parameters even in small quantities. Fig. 2 shows the results of an example of automatic detection of central feature points using commercial software.

The random sample consensus (RANSAC) method can effectively remove the outliers in the point cloud and has more applications in point cloud processing [44]. However, the RANSAC method is basically implemented based on a functional model, which could be overwhelming when faced with a stochastic model. Therefore, we draw on the general principle of robust estimation, which is more commonly used in geodesy, to deal with this problem. The basic idea is to use the equivalence weight principle to reduce the weight of gross errors, so as to reduce their deteriorations in the parameters solution process.

The weight matrix in the estimation criterion at this point will be replaced by the general equivalence weight matrix $\bar{\mathbf{P}}$ as follows:

$$\mathbf{V}^{\mathrm{T}}\bar{\mathbf{P}}\mathbf{V} = \min \tag{33}$$

where

$$\bar{\mathbf{P}} = \begin{bmatrix}\bar{\mathbf{P}}_1 & \\ & \bar{\mathbf{P}}_2\end{bmatrix} = \begin{bmatrix}\bar{\mathbf{Q}}_1^{-1} & \\ & \bar{\mathbf{Q}}_2^{-1}\end{bmatrix} = \bar{\mathbf{Q}}^{-1}. \tag{34}$$

$\bar{\mathbf{P}}_1$ and $\bar{\mathbf{P}}_2$ are equivalent weight matrices of the original observations of TS and TLS, respectively; and $\bar{\mathbf{Q}}_1$ and $\bar{\mathbf{Q}}_2$ are the corresponding equivalent cofactor matrices. The method of gross errors' rejection using robust estimation is essentially the same as the derivation process described above, except that the weight matrix (or cofactor matrix) need be replaced with an equivalent weight matrix (or equivalent cofactor matrix).

The equivalent weight matrix can be calculated by the weight factor function, and here we used the IGG III weight factor function, whose inverse is the factor function of the corresponding cofactor matrix. The IGG III cofactor function realized via a three-stage approach [43], [45], that is, the normal part retains the original weights, the available part reduces the weights of the observations, and the rejection part eliminates the gross error by assigning zero value to the weights of the observations:

$$F_n = \begin{cases} 1.0 & |\tilde{e}_n| \le k_0 \\ \frac{|\tilde{e}_n|}{k_0}\left(\frac{k_1-k_0}{k_1-|\tilde{e}_n|}\right)^2 & k_0 < |\tilde{e}_n| \le k_1 \\ 10^{10} & k_1 < |\tilde{e}_n| \end{cases} \tag{35}$$

where n denotes the index number of matrix elements; k_0 and k_1 are the thresholds, and according to [46]–[48], the ranges of k_0 and k_1 are 2.0–3.0 and 4.5–8.5, respectively. In the third part, $k_1 < |\tilde{e}_n|$, the observations are considered to incorporate gross errors, and its equivalent weight factor is 0 in theory, i.e., the cofactor should be infinite. For the purpose of computational convenience and to meet practical requirements, we replaced it with an extreme value (10^{10}) instead. $\tilde{e}_n$ denotes the normalized residuals, and

$$\tilde{e}_n = \frac{e_n}{\sigma_0\sqrt{Q_{e_n}}}, \quad Q_{e_n} \neq 0. \tag{36}$$

Here, e_n is a single element in the residual vector; Q_{e_n} is the nth element on the main diagonal of the residual covariance matrix; and σ_0 denotes the unit weight medium error, which can be calculated by the median function [46]:

$$\sigma_0 = \mathrm{median}\left(|e_n/Q_{e_n}|\right) \times 1.4826, \quad Q_{e_n} \neq 0. \tag{37}$$

The standardized residual vector can better reflect the abnormal information in the observation vector, and when there are gross errors in the observations, the abnormal information will be reflected in the residual vector in time to avoid the contamination of the results, ensuring the reliability of the results [49]. In addition, the IGG III function is constructed using normalized residuals, which can effectively consider the influence of observation space and design space on parameter valuation [48].

Since the observations used in this article are distances and angles rather than 3-D Cartesian coordinates, the observations are considered to be independent of each other, so the equivalent covariance matrix can be obtained by

$$\bar{\mathbf{Q}}_n = \mathbf{Q}_n F_n. \tag{38}$$

It is worth stating that if there is correlation between observations, the equivalence cofactor matrix can be computed in the form of a two-factor model to maintain the original correlation between the observed values, which can be found in [43], [46], [47]. It should be noted that in order to achieve the aim of resistance, the equivalent cofactor matrix needs to be updated continuously during the iterative calculation [40], [41], [47], [50].

D. Derivation of Residual Covariance Matrix

The key to robust estimation of parameters based on the principle of equivalent weight matrix is the derivation of the covariance matrix of the residual vector. According to (31), the estimated residual errors after the *j*th iteration can then be expressed as

$$\tilde{\mathbf{e}} = \begin{bmatrix} \tilde{\mathbf{e}}_1 \\ \tilde{\mathbf{e}}_2 \end{bmatrix} = \begin{bmatrix} \mathbf{M}^j \\ \mathbf{N}^j \end{bmatrix} \mathbf{G}^j \tag{39}$$

where

$$\begin{cases} \mathbf{M}^j = -\mathbf{Q}_1^j \left(\mathbf{A}_1^j\right)^{\mathrm{T}} \left(\mathbf{Q}_c^j\right)^{-1} \\ \mathbf{N}^j = \mathbf{Q}_2^j \left(\mathbf{A}_2^j\right)^{\mathrm{T}} \left(\mathbf{Q}_c^j\right)^{-1} \\ \mathbf{G}^j = \mathbf{L}^j - \mathbf{B}^j \mathrm{d}\hat{\xi}^{j+1}. \end{cases} \tag{40}$$

Since all observations in the matrices $\mathbf{M}^j$, $\mathbf{N}^j$, and $\mathbf{G}^j$ are approximations, the traditional application of the covariance propagation method cannot achieve the derivation of the residual covariance matrix directly. Whereas, by analyzing (20), (26), and (27), it can be found that

$$\mathbf{L}^j - \mathbf{B}^j d\xi = -\mathbf{A}_1^j \mathbf{e}_1 + \mathbf{A}_2^j \mathbf{e}_2 = \begin{bmatrix} -\mathbf{A}_1^j & \mathbf{A}_2^j \end{bmatrix} \begin{bmatrix} \mathbf{e}_1 \\ \mathbf{e}_2 \end{bmatrix} = \mathbf{J}\mathbf{V}. \tag{41}$$

Here, $\mathbf{J}^j = [-\mathbf{A}_1^j \ \mathbf{A}_2^j]$. Hence, the covariance matrix of $\tilde{\mathbf{V}}$ could be calculated using *a priori* information. Integrating (39)–(41) and associating with (25), the covariance matrix of residuals according to the covariance propagation algorithm can be expressed as

$$\mathbf{Q}_e = \begin{bmatrix} \mathbf{M}^j \\ \mathbf{N}^j \end{bmatrix} \underbrace{\mathbf{J}^j \mathbf{Q} \left(\mathbf{J}^j\right)^{\mathrm{T}}}_{\mathbf{Q}_G} \begin{bmatrix} \left(\mathbf{M}^j\right)^{\mathrm{T}} & \left(\mathbf{N}^j\right)^{\mathrm{T}} \end{bmatrix}. \tag{42}$$

Furthermore, since the 3-D coordinates need to be converted to the original observations in the self-calibration model, which invariably increases the types of observations from one to two, it is theoretically uncritical to use the same *a priori* medium error. For this problem, the correct treatment should be based on the idea of VCE to unify the medium errors of different classes of observations, determining a reasonable weight ratio of different classes of observations, and then adopt the proposed method to resist the effect of gross errors.

While the elements of the coefficient matrix and the observation vector do not belong to the same class of observations, they often do not belong to the same order of magnitude in terms of accuracy, and the definition of the stochastic model is biased. In practice, the initial covariance matrices (or weight matrices) are often not accurately given, or the unit weight variances corresponding to the various types of observations are not consistent. It is therefore particularly significant to improve the leveling results by reweighting the various observations using *a posteriori* information (e.g., residual vectors, etc.). In this case, it is obviously unreasonable to determine the weights of the observations uniformly by a single medium error [34]–[36], [51]. The VCE algorithm can better achieve the problem of weighting when multiple classes or multiple accuracy observations are adjusted together, but if the observations contain gross errors, the effects would be transferred to the stochastic model and the results are thus often inaccurate and could not conduct the optimal parameter valuations, in other words, the valuation of variance components could be distorted.

In case of outliers, its influences on the valuation of the variance components can be attenuated by means of robust estimation. Besides, the ranges of available values of residuals are different for different observation distributions, and it is also necessary to normalize each type of residuals separately for different types of observations in order to maintain the equilibrium under the mixed turntable [52]. Specifically, in the process of calculating the median for robust estimation, the respective medians can be calculated according to the classification of the observations to ensure the applicability of the results, taking into account the different *a priori* information for each type of observation.

The index of the matrix elements in the functional and stochastic models needs to be reordered according to the classification of observations to satisfy the requirements of VCE theory before the calculation. The reordering of matrix elements can have various forms, and depending on the ordering, one of them can be found in Appendix A of [2]. However, it should be clarified that the left-hand side of the functional model, i.e., (6), does not need to be converted from Cartesian coordinates to the original observations if VCE is not employed, and the error propagation law can then be introduced for determining the weights.

TABLE I
TRUE VALUES OF PARAMETERS

EOPs	Values	CPs	Values
Δx(m)	10	m(m)	0.004
Δy(m)	5	λ	0.0001
Δz(m)	10	c(rad)	0.0001
φ(rad)	0.5	i(rad)	0.001
ω(rad)	0.5	t(rad)	–0.0001
κ(rad)	1.0		

TABLE II
STANDARD DEVIATION OF ORIGINAL OBSERVATIONS

TLS	Values	TS	Values
s(m)	0.005	ρ(m)	0.002
θ(μrad)	73	γ(μrad)	24
α(μrad)	73	β(μrad)	24

TABLE III
SIMILARITIES AND DIFFERENCES OF THE SCHEMES

Schemes	Random errors of TS	Random errors of TLS	CPs	Gross errors
1	×	×	√	×
2	×	√	√	×
3	√	√	√	√

It is certainly feasible to use the 3-D Cartesian coordinates for the left-hand side of the functional model, while the corresponding covariance or weight matrix of the left-hand side will need to be changed accordingly, which can be achieved by means of the variance covariance propagation law; similarly, the residual vector and its associated coefficient matrix will be adjusted during the above iterations, taking into account the update of the observed values and the unknown parameters.

E. Iterative Calculation Process

In accordance with the above theoretical and derivative procedure, the unknown parameters and the random errors of the two coordinate systems can be decomposed. For the reader's convenience and understanding, the specific iterative calculation process can be represented as follows:

1. Calculate the Original Observations of the Common Points: Since the proposed method uses distances and angles, it is necessary, according to (1), to convert the 3-D Cartesian coordinates acquired by the scanner to the original observations. To ensure the correctness of the conversion result, (2) can be employed for collation and validation.

2. Obtain the Initial Values of the Unknown Parameters and Random Errors: As the initial values do not need to be perfectly accurate, assuming that the instruments are in an ideal state during the observation and scanning sweeps, therefore the systematic error terms and random errors can be deemed to be 0. The remaining EOPs can be obtained according to the linear Bulsa–Wolf model, or solved according to [4]. Of course, more precise initial values can reduce the iterations to some extent and improve the efficiency of the operations, which can then be carried out by the nonlinear equation (4).

3. Iterative Process:

1) Deciding the observation residuals of the jth iteration (where the results of the first iteration are calculated using the initial values) according to the WTLS principle, using a linearized functional model, and a stochastic model defined by nominal accuracy, i.e., (15) and (23), until the parameter offsets are less than a set threshold.
2) Substituting the predicted values of the residual vector $\tilde{\mathbf{e}}$and its corresponding cofactor matrix $\boldsymbol{Q}_e$ into (35)–(37) and calculating the standardized residuals for the jth iteration by classifying the residuals according to the observations, respectively.
3) Implementing an equivalent cofactor matrix for the observations based on the cofactor factors and the initial cofactor matrix, using (38).
4) Calculating the parameter estimates for the $(j+1)$th iteration and updating the residuals of the observations according to the principle of equivalent weights.
5) Reestimating the residual cofactor matrix together with (39)–(42) and the *a priori* information on the observations.
6) Return to step (2) until the iteration stop condition is reached.
7) Reweighting the observations following the estimation of the residuals, using the method in [51] for the estimation of the variance components.
8) Return to step (1) until the variance components of each class of observations are less than the given threshold and stop iterating.

4. Accuracy Evaluation.

IV. EXPERIMENTS AND ANALYSIS

In a bid to verify the effectiveness and robustness of the method, it was investigated at both algorithm and model levels without considering the network design and measurement configuration. Experiments were conducted using simulated and measured data, and the overall experimental idea was to observe concrete target points at specified locations using a TS with high accuracy and a TLS to be calibrated. After two sets of Cartesian observations located in two coordinate systems were obtained, the data series were meant to be converted into original observations according to the scanner observation principle, after which the CPs and EOPs would be computed by means of different self-calibration methods or models, and the respective experimental results attained were logically compared and analyzed.

A. Data Simulation

By assuming that a random distribution of 40 target points is spread over a scanning volume, a distribution of target points is generated in accordance with the true FOV of the instrument, whereby the distances from the target points to the center of the scanning geometry are set from 10 to 30 m; the vertical perspectives are pitched from $-45°$ to 90°; and the horizontal

TABLE IV
RMSE FOR UNKNOWN PARAMETERS WHEN THE NUMBER OF GROSS ERROR IS 0

Schemes	EOPs							CPs			
	Δx(m)	Δy(m)	Δz(m)	φ(rad)	ω(rad)	κ(rad)	m(m)	λ	c(rad)	i(rad)	t(rad)
1	7.4889×10^{-4}	7.9497×10^{-4}	0.0016	2.8287×10^{-5}	2.3740×10^{-5}	2.6463×10^{-4}	0.0033	2.2524×10^{-4}	2.3790×10^{-4}	4.6128×10^{-5}	9.5658×10^{-5}
2	4.2697×10^{-4}	4.6114×10^{-4}	6.7196×10^{-4}	2.7400×10^{-5}	2.4500×10^{-5}	2.8588×10^{-4}	0.0032	2.2335×10^{-4}	2.5517×10^{-4}	4.9700×10^{-5}	4.4500×10^{-5}
3	2.9688×10^{-4}	3.2578×10^{-4}	5.4577×10^{-4}	2.2659×10^{-5}	2.1457×10^{-5}	2.0827×10^{-4}	0.0032	2.2186×10^{-4}	1.8770×10^{-4}	3.8194×10^{-5}	4.2099×10^{-5}

TABLE V
RMSE FOR UNKNOWN PARAMETERS WHEN THE NUMBER OF GROSS ERROR IS 1

Schemes	EOPs							CPs			
	Δx(m)	Δy(m)	Δz(m)	φ(rad)	ω(rad)	κ(rad)	m(m)	λ	c(rad)	i(rad)	t(rad)
1	0.0013	0.0014	0.0028	5.8700×10^{-5}	4.5728×10^{-5}	5.4920×10^{-4}	0.0051	3.5281×10^{-4}	5.0214×10^{-4}	8.6490×10^{-5}	1.7387×10^{-4}
2	5.6834×10^{-4}	5.0562×10^{-4}	9.3995×10^{-4}	5.5390×10^{-5}	3.6177×10^{-5}	4.8221×10^{-4}	0.0050	3.5245×10^{-4}	4.3653×10^{-4}	8.0447×10^{-5}	7.1006×10^{-5}
3	3.3890×10^{-4}	3.1179×10^{-4}	5.0838×10^{-4}	3.0484×10^{-5}	2.0741×10^{-5}	2.7167×10^{-4}	0.0029	2.0495×10^{-4}	2.4548×10^{-4}	4.6552×10^{-5}	3.9245×10^{-5}

TABLE VI
RMSE FOR UNKNOWN PARAMETERS WHEN THE NUMBER OF GROSS ERROR IS 3

Schemes	EOPs							CPs			
	Δx(m)	Δy(m)	Δz(m)	φ(rad)	ω(rad)	κ(rad)	m(m)	λ	c(rad)	i(rad)	t(rad)
1	0.0022	0.0022	0.0042	8.2195×10^{-5}	8.1907×10^{-5}	6.1025×10^{-4}	0.0080	6.1091×10^{-4}	5.5165×10^{-4}	1.3518×10^{-4}	2.8627×10^{-4}
2	6.6359×10^{-4}	6.5452×10^{-4}	0.0011	6.1974×10^{-5}	6.0701×10^{-5}	5.7439×10^{-4}	0.0080	6.0745×10^{-4}	5.2741×10^{-4}	1.2509×10^{-4}	9.9471×10^{-5}
3	3.5337×10^{-4}	3.6963×10^{-4}	4.9719×10^{-4}	2.7577×10^{-5}	2.7441×10^{-5}	3.4252×10^{-4}	0.0031	2.3672×10^{-4}	3.2558×10^{-4}	9.0820×10^{-5}	4.3579×10^{-5}

TABLE VII
RMSE FOR UNKNOWN PARAMETERS WHEN THE NUMBER OF GROSS ERROR IS 5

Schemes	EOPs							CPs			
	Δx(m)	Δy(m)	Δz(m)	φ(rad)	ω(rad)	κ(rad)	m(m)	λ	c(rad)	i(rad)	t(rad)
1	0.0030	0.0028	0.0054	9.2672×10^{-5}	1.3999×10^{-4}	9.5331×10^{-4}	0.0110	8.3617×10^{-4}	8.3896×10^{-4}	1.8311×10^{-4}	4.0696×10^{-4}
2	7.4045×10^{-4}	8.5507×10^{-4}	0.0015	7.6054×10^{-5}	8.8861×10^{-5}	7.1750×10^{-4}	0.0108	8.2385×10^{-4}	6.4192×10^{-4}	1.2822×10^{-4}	1.3857×10^{-4}
3	3.5348×10^{-4}	3.7963×10^{-4}	5.5243×10^{-4}	2.4286×10^{-5}	3.4382×10^{-5}	3.4381×10^{-4}	0.0034	2.6591×10^{-4}	3.1673×10^{-4}	6.4860×10^{-5}	4.8182×10^{-5}

perspectives range from 0° to 360°. Beginning with the given true values (TV) for the TLS and parameters, one first derives the corresponding TV of TS according to the proposed functional model, and then adds random errors to the TV by simulating the respective *a priori* information. The TV, that is, ξ_{true} of EOPs and CPs were generated according to the actual instrument parameters, as shown in Table I.

Thirty points were randomly selected as common points, and the remaining ones were naturally regarded as check points. Under the standard zero assumption condition, the standard deviations of all the original TS and TLS observations are given in Table II, referring to the true nominal information of Leica HDS3000 and SOKKIA NET1200.

Throughout the simulation of random errors, we assumed that as they obey a normal distribution, all the original observations should be uncorrelated. Gross errors emerged at arbitrary locations (any one observation is possible, even in all three components of a point at the same time) and were 5–20 times the size of the standard deviation [46]. A total of 2000 simulations were then carried out with the number of gross errors at 0, 1, 3, and 5, respectively.

B. Simulated Data Calculation Results

Based on the simulated experimental data, the schemes were envisaged as as follows:

Scheme 1: Method considering only systematic errors but ignoring all random errors [4], [10], [20], [31], i.e., the lower part of (4).

Scheme 2: Calibration method in view of random errors in TLS observations and VCE without taking gross errors into account, for instance [2], [21].

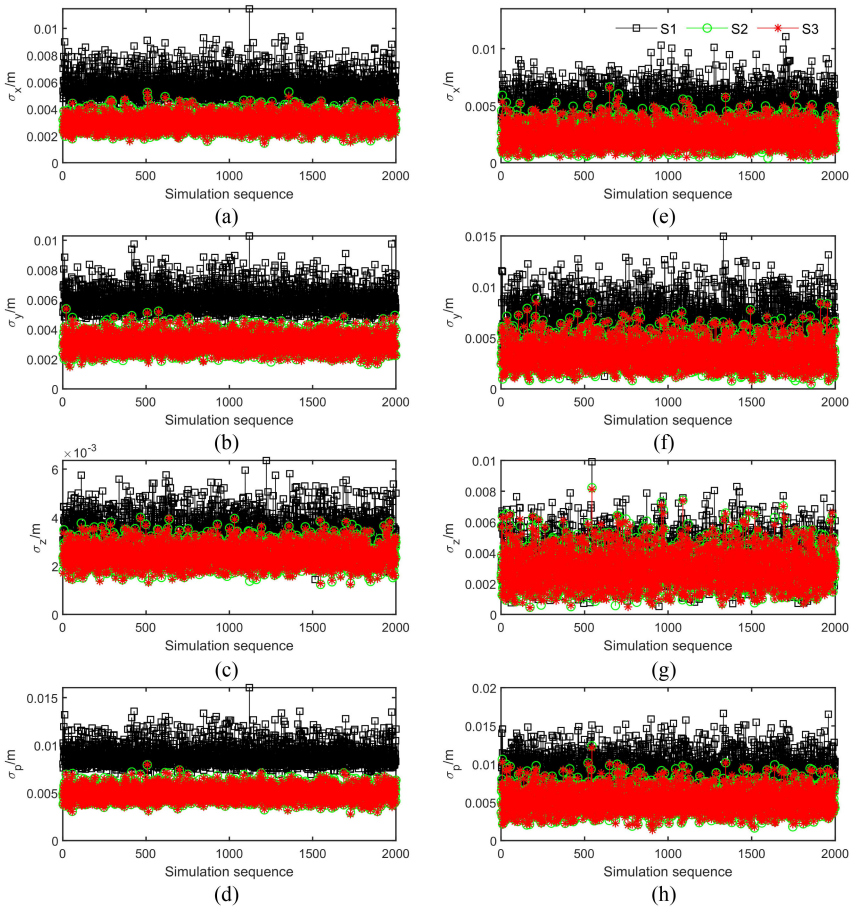

Fig. 3. Medium errors of homonymous and check points when the number of gross errors is 0. (a) Medium errors of homonymous points in x direction. (b) Medium errors of homonymous points in y direction. (c) Medium errors of homonymous points in z direction. (d) Medium errors of homonymous points. (e) Medium errors of checkpoints in x direction. (f) Medium errors of check points in y direction. (g) Medium errors of check points in z direction. (h) Positional medium errors of check points.

Scheme 3: Method proposed in this article.

Combining the above experimental methods, the various categories of parameters and errors considered in all the schemes were distinguished and classified in order to facilitate the identification of similarities and differences across the schemes, as shown in Table III.

In the calculation process, the initial values of the parameters of Scheme 1 are calculated using a linear coordinate transformation model that has a similar form with the upper part of (4). To ensure the efficiency of the operation and the correctness of the initial values of the iterations, the calculation results of Scheme 1 are then treated as the initial values of the unknown parameters of the remaining schemes.

Due to the small values of standard deviation of the two instruments, the *a priori* unit power medium error was set to $\sigma_0 = 10^{-8}$ to ensure the efficiency and the number of valid bits of the elements of the weight matrices and also cofactor matrices, allowing for too large a gap between the *a priori* information on distance and angle observations. Once the iterative calculation has been accomplished, the original observations of the TLS would be corrected against the estimated CPs and converted to the coordinate system of the TS via EOPs. Based on the TVs of the target points of the TS and the corrected TLS coordinates, the coordinate component errors $(\sigma_x, \sigma_y, \sigma_z)$ and point median error σ_p of the homonymous points are calculated to evaluate the results and accuracy of the self-calibration:

$$\begin{cases} \sigma_x = \sqrt{\sum_{l=1}^{30} (x_c - x_{\text{ts}})^2 / 30} \\ \sigma_y = \sqrt{\sum_{l=1}^{30} (y_c - y_{\text{ts}})^2 / 30} \\ \sigma_z = \sqrt{\sum_{l=1}^{30} (z_c - z_{\text{ts}})^2 / 30} \\ \sigma_p = \sqrt{\sigma_x^2 + \sigma_y^2 + \sigma_z^2} \end{cases} \tag{43}$$

where (x_c, y_c, z_c) denote the corrected Cartesian coordinates of TLS via the solved parameters in TS frame; and l represents the index of the coordinate value within the sequence.

The accuracy of the check points could be evaluated in the same way, but the denominator needs to be changed to the quantity of check points. In addition, given the presence of the TVs of the parameters in the simulation data, the offset $\nabla\xi$ and root mean square error (RMSE) of the parameter estimates apart

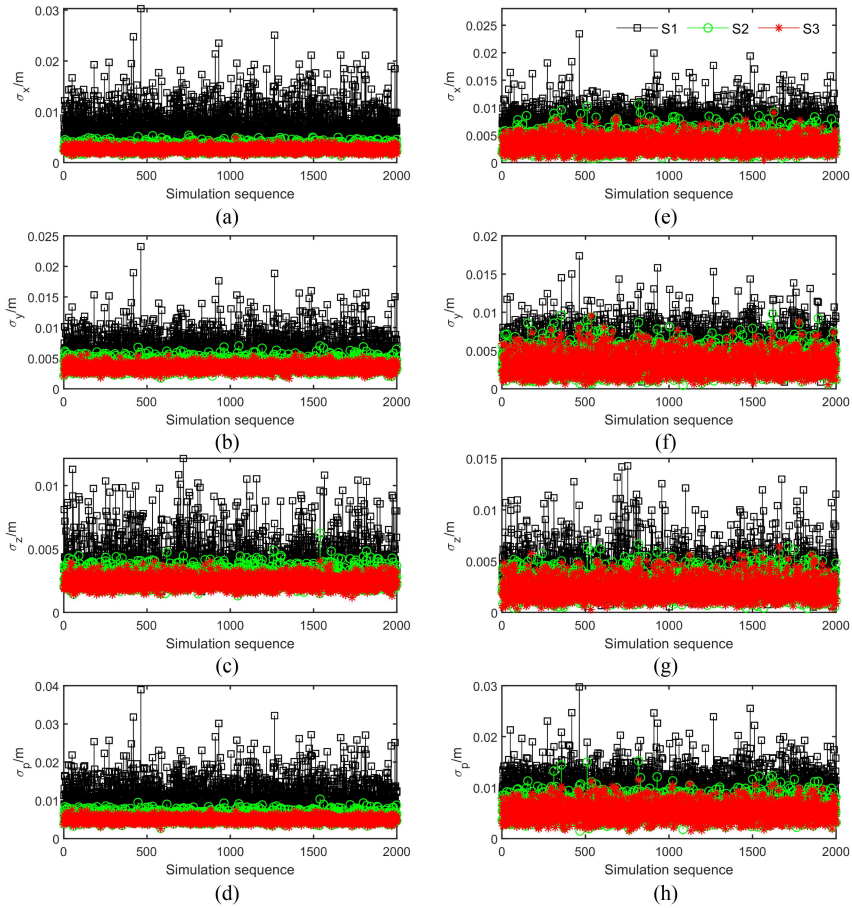

Fig. 4. Medium errors of homonymous and check points when the number of gross errors is 1. (a) Medium errors of homonymous points in x direction. (b) Medium errors of homonymous points in y direction. (c) Medium errors of homonymous points in z direction. (d) Medium errors of homonymous points. (e) Medium errors of checkpoints in x direction. (f) Medium errors of check points in y direction. (g) Medium errors of check points in z direction. (h) Positional medium errors of check points.

TABLE VIII
STANDARD DEVIATION OF ORIGINAL OBSERVATIONS

TLS	Values	TS	Values
s(m)	0.005	ρ(m)	0.002
θ(μrad)	17	γ(μrad)	14
α(μrad)	17	β(μrad)	14

from the TVs were then employed to verify the quality as well:

$$\begin{cases} \nabla\xi = \tilde{\xi} - \xi_{\text{true}} \\ \text{RMSE} = \sqrt{\sum_{j=1}^{2000} (\nabla\xi)^2 / 2000} \end{cases} \tag{44}$$

where $\tilde{\xi}$ and ξ_{true} are the predicted values and TVs of the parameter vector, respectively; and j is the index of the simulation.

Statistics on the computed outcomes of 2000 simulations in conjunction with (30) and (44) yield the following RMSE of each parameter for the case of different amounts of gross errors, as shown in Tables IV–VII. On the other hand, the coordinate components and point accuracy of the homonymous and check points obtained according to (43) are shown in Figs. 3–6. To save spaces, we used "S" instead of "Scheme" in the legends in the following figures.

In view of facilitating the reader's reading and understanding, as well as for a more intuitive display, we also plotted the offset and RMSE for each parameter, and the relevant results can be found in the Appendix A.

Alternatively, to validate the stability and robustness of the proposed method, cross-sectional statistics and comparisons of the RMSEs of the parameters calculated under different conditions of the number of gross errors are as well demanded. Thus, we adapted the coordinates of the check points together with the TS truth values, as shown in Table I, taking into account the given parameters of TV and calculating their coordinate component errors and pointwise errors at different numbers of gross errors (NG), and presenting the corresponding results in Fig. 7, in contrast to Scheme 3 and Scheme 4. For the simulation data, it is straightforward to find out the following conditions from Tables IV to VII, Figs. 3 to 7, as well as Figures in Appendix A:

1) When the number of coarse deviations is 0, i.e., all coordinates contain only random errors as well as systematic errors (in the case of TLS), the results of Scheme 1 (black lines) compare least favorably, mainly because the random errors of observations and the effect of the stochastic

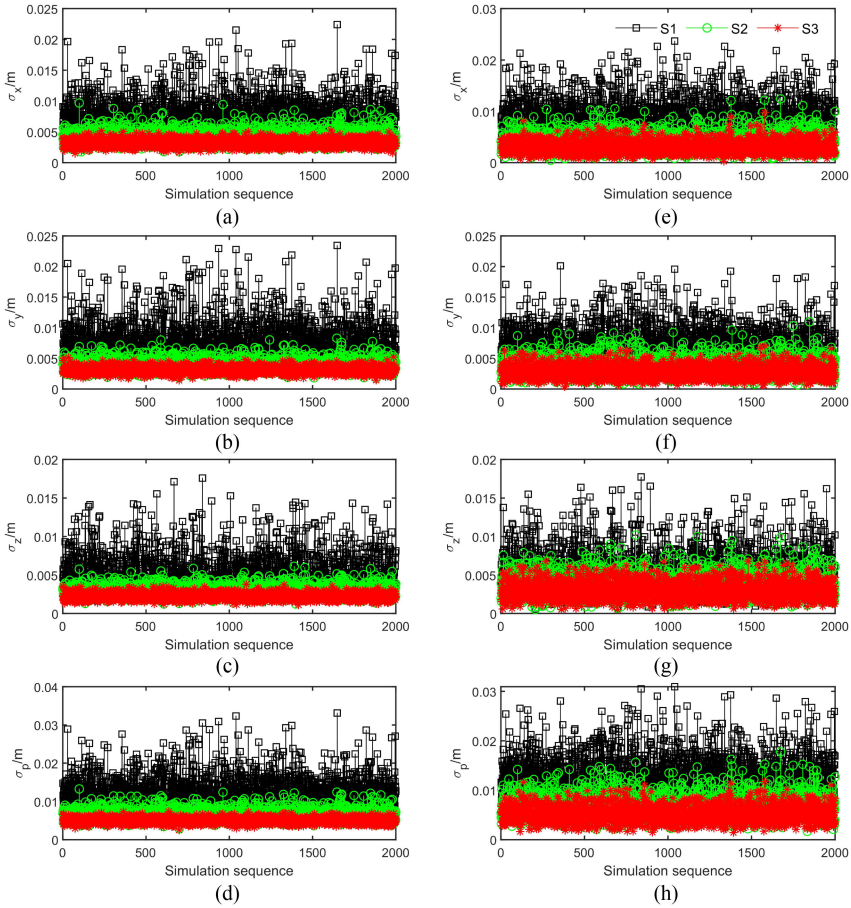

Fig. 5. Medium errors of homonymous and check points when the number of gross errors is 3. (a) Medium errors of homonymous points in x direction. (b) Medium errors of homonymous points in y direction. (c) Medium errors of homonymous points in z direction. (d) Medium errors of homonymous points. (e) Medium errors of checkpoints in x direction. (f) Medium errors of check points in y direction. (g) Medium errors of check points in z direction. (h) Positional medium errors of check points.

TABLE IX
ACCURACY OF CHECKPOINTS

Schemes	σ_x(m)	σ_y(m)	σ_z(m)	σ_p(m)
1	0.0111	0.0087	0.0076	0.0161
2	0.0093	0.0046	0.0077	0.0129
3	0.0071	0.0052	0.0051	0.0101
4	0.0053	0.0039	0.0016	0.0068

model on parameter estimation are neglected; in contrast to Scheme 2 (green lines), which introduced the TLS random errors, Scheme 3 (red lines) also incorporated the random errors of TS, which, despite its small values, gives slightly better results than Scheme 2 in parameter estimation and point accuracy evaluation.

2) While the coarse deviations are present, the RMSE of the parameters solved by Scheme 3 are closer to zero compared to schemes 1 and 2, namely, the accuracies of all parameters are improved and the corrections of the coordinates using the settlement values are closer to the TVs of the reference coordinates.
3) As the number of gross errors increases, the parameter RMSE of Scheme 1 and Scheme 2 continuously increased, indicating that these two methods are more sensitive to coarse deviations. Scheme 3, on the other hand, can maintain stable RMSE of the parameters, suggesting the robustness and effectiveness of the proposed method, with the addition constant m being particularly evident. Taking the case when the quantity of coarse observations is 5, the accuracies of CPs are, respectively, improved by 68%, 68%, 51%, 49%, and 65% in Scheme 3 compared with Scheme 2, according to the index of CPs in the parameter vector; the accuracies of EOPs are as well augmented, hovering at 60%.
4) However, it is undeniable that there are some points in the check points where Scheme 3 has slightly inferior component and position errors than Scheme 2, which is not unusual and is mainly dominated by the TLS random errors.
5) In addition, we also corrected and transformed the checkpoint coordinates using the TVs of the given parameters, and compared them with Scheme 2 and Scheme 3, as shown in Fig. 6. When the volume of coarse observations

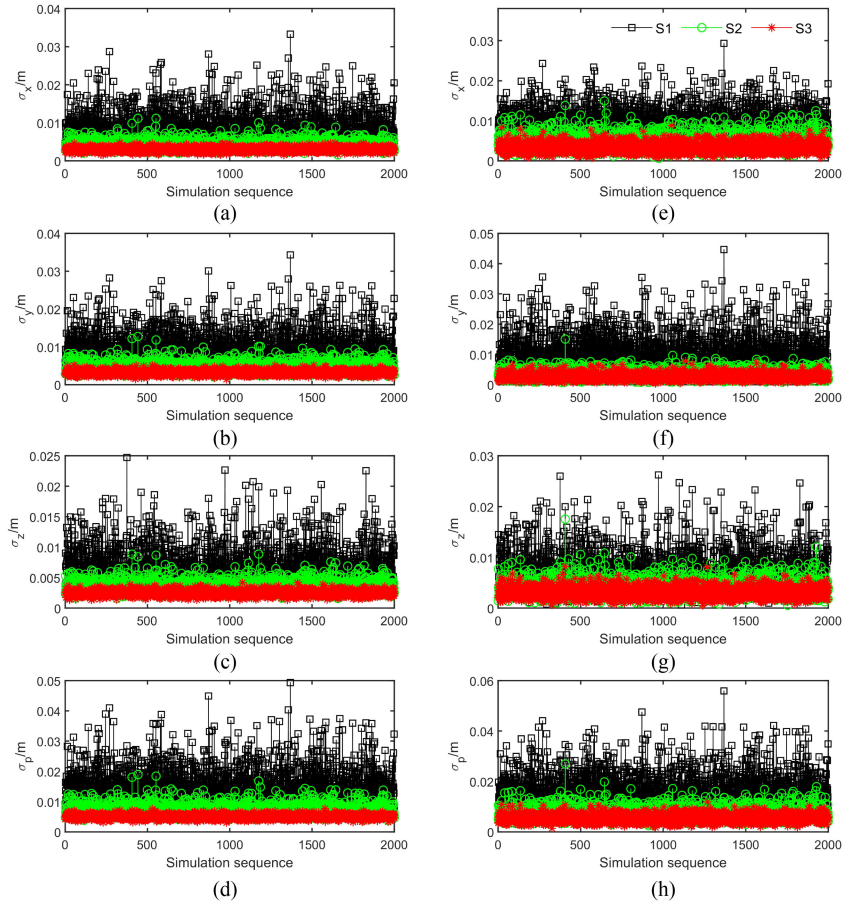

Fig. 6. Medium errors of homonymous and check points when the number of gross errors is 5. (a) Medium errors of homonymous points in x direction. (b) Medium errors of homonymous points in y direction. (c) Medium errors of homonymous points in z direction. (d) Medium errors of homonymous points. (e) Medium errors of checkpoints in x direction. (f) Medium errors of check points in y direction. (g) Medium errors of check points in z direction. (h) Positional medium errors of check points.

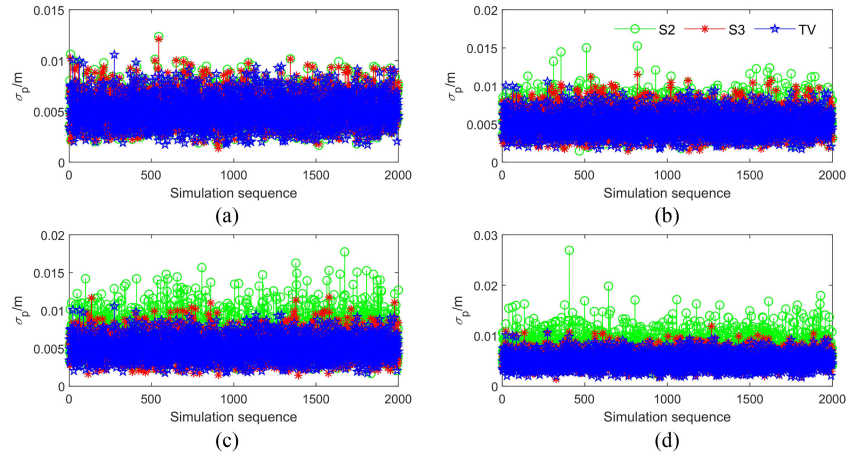

Fig. 7. Medium errors of check points in position at various quantities of gross errors. (a) NG = 0. (b) NG = 1. (c) NG = 3. (d) NG = 5.

is 0, the variations in are generally not significant; however, as the number of gross errors proceeds, an identical trajectory to the TV results can only be maintained for scenario 3.

C. Measured Data

With a view to validating the effectiveness and robustness of the proposed method in practice, a quantitative evaluation was carried out. To attenuate the possible correlations among

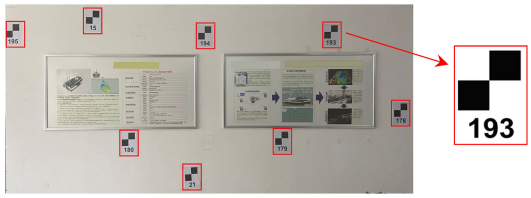

Fig. 8. Distribution of a part of the points.

unknown parameters, 33 flat paper targets were placed nonuniformly on the wall and roof in a selected laboratory, and each flat target (a square with a dimension of 2 × 2) consisted of four adjacent squares in black and white separately with the center point considered as a target. The 3-D coordinates of the target centroids were recorded by the Leica TS02 Plus TS (while recording the original observations for verification) as reference coordinates and the extraction of the point cloud obtained from the HS650i TLS, individually. The distance between every settled target and the geometric center of TLS were about 6.5 m; the scope of horizontal angles belongs to 0°–360°; the range of vertical angles is –40°–60°. A partial distribution of the points is displayed in Fig. 8 .

Prior to the calculation, we performed a coarse alignment of the two sets of coordinates, on the one hand to determine the index of the coarse observations, excluding the coarse coordinates from appearing in the check points affecting the subsequent accuracy assessment, and also to make a preliminary estimate of the magnitude of the coarse deviations. Taking the TS coordinates as a benchmark, we found that three points in the TLS data had a deviation of 1–3 cm in the x-direction (No. 5, 14, and 20); No. 20 had a deviation of 5 cm in the y-direction, and 2 cm in the z-direction at No. 16. In addition, we had proactively added a 10 cm deviation in the x-coordinates of No. 6 and 12 to describe how it behaves when the gross errors are very large.

Except for the points containing coarse errors, eight points were randomly selected as check points among the remaining available, while the rest points were considered as homonymous. The nominal accuracy of the instrument was regarded as a priori information (see Table VIII for details) to weight the original observations.

After conversion to international units, the value of the error in the *a priori* unit weight σ_0 was determined to 10^{-8} here as well. On the other hand, compared with the simulation experimental schemes, we additionally introduced a coordinate transformation method based on Gauss–Markov model, i.e., only EOPs without CPs in the unknown parameter vector, to analyze the effectiveness of CPs for coordinate corrections. The corresponding experimental schemes are designed as follows:

Scheme 1: Traditional coordinate transformation method based on Gauss–Markov model without considering systematic errors, the upper part of (4).

Scheme 2: Method considering only systematic errors but ignoring all random errors.

Scheme 3: Method in view of Gauss–Helmert model and VCE without considering gross errors.

Scheme 4: Method proposed in this article.

On the basis of (43), the coordinate component error and the error in point position can be calculated for each check point, which is however modified here by the quantity of check points in the denominator, and the results are shown in Table IX.

From the computation of the measured data, we can conclude the following:

1) Scheme 1 has the absolute lamest results, which demonstrates that a reasonable and correct instrument calibration can effectively weaken the effect of CPs on the coordinate sequence and improve the accuracy of the coordinate data, as has been described in numerous publications.
2) The proposed method can improve the point accuracy from centimeter to millimeter level; compared to the other three methods, the accuracy of check points could be enhanced by 58%, 47%, and 33%, respectively.
3) In fact, we have also calculated the component and point accuracy of the homonymous points and the proposed method is still optimal compared to the first three methods, so the proposed method can still achieve the best fit to the model in the presence of gross errors.

V. Conclusion

Theoretically, the function model cannot achieve a perfect fitting when there are coarse deviations in the observations, which means that the model may be erroneous at this point. In this article, a robust target-based TLS self-calibration method has been proposed on the basis of the Gauss–Helmert model, which took into account the random errors present in both TS and TLS observations in the functional model. In terms of the stochastic model, we introduced VCE posterior estimates for the discrepancy between angular and ranging accuracy and reweight the coarse observations by constructing an equivalent covariance matrix from the standardized residuals.

Through the validation of the simulated and measured data, it can be found that the coordinate components and position accuracy can be effectively improved after manipulating using the proposed method; on the other hand, the estimated values of the parameters are closer to the TVs in the simulation data, and it could maintain satisfactory parameter vector stability and robustness as the quantity of coarse observations increases. Although the accuracy of a very small number of checkpoints is marginally inferior to that of the traditional methods, mainly due to the random errors of the check points, this neither determined the effectiveness of the proposed method qualitatively. Therefore, irrespective of the presence or absence of coarse differences (within reasonable limits), the proposed method was not only effective in estimating the unknown parameters, but in addition the random errors in the observations can be evaluated reasonably well. In theory, it is more rigorous and reasonable than the ordinary self-calibration methods. In addition, apart from systematic error self-calibration, the algorithm in this article can also be applied to solve some other problems, for instance, point cloud registration, coordinate transformation, image processing, etc.

Admittedly, there would be some loss of efficiency in the new method due to the employment of *a posteriori* estimation,

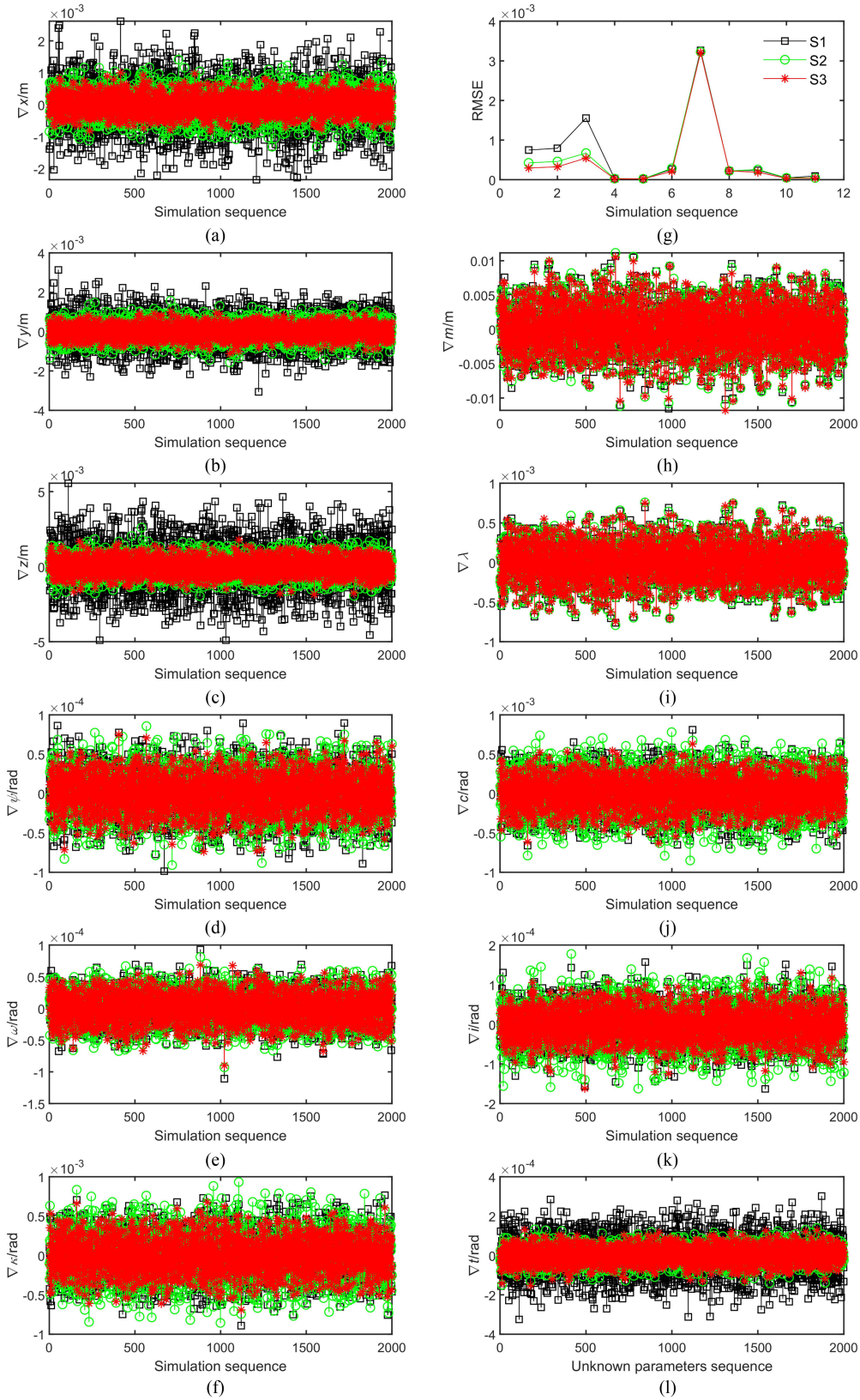

Fig. 9. Deviations of the parameters and their RMSE when the number of gross errors is 0: (a)∇x; (b)∇y; (c)∇z; (d)$\nabla \varphi$; (e)$\nabla \omega$; (f)∇k; (g) RMSE of parameters; (h)∇m; (i)$\nabla \lambda$; (j)∇c; (k)∇i; and (l)∇t.

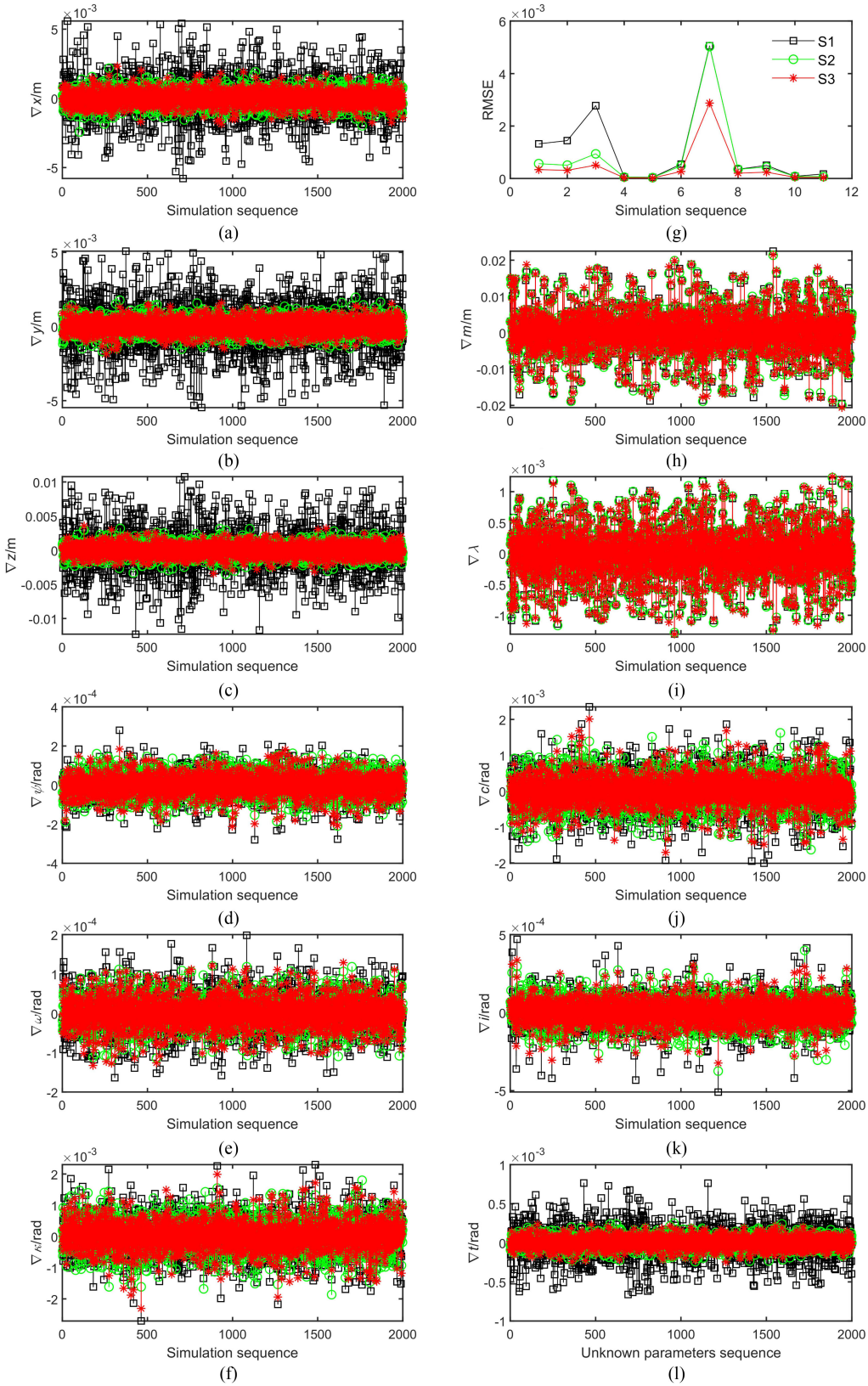

Fig. 10. Deviations of the parameters and their RMSE when the number of gross errors is 1: (a)∇x; (b)∇y; (c)∇z; (d)$\nabla \varphi$; (e)$\nabla \omega$; (f)∇k; (g) RMSE of parameters; (h)∇m; (i)$\nabla \lambda$; (j)∇c; (k)∇i; and (l)∇t.

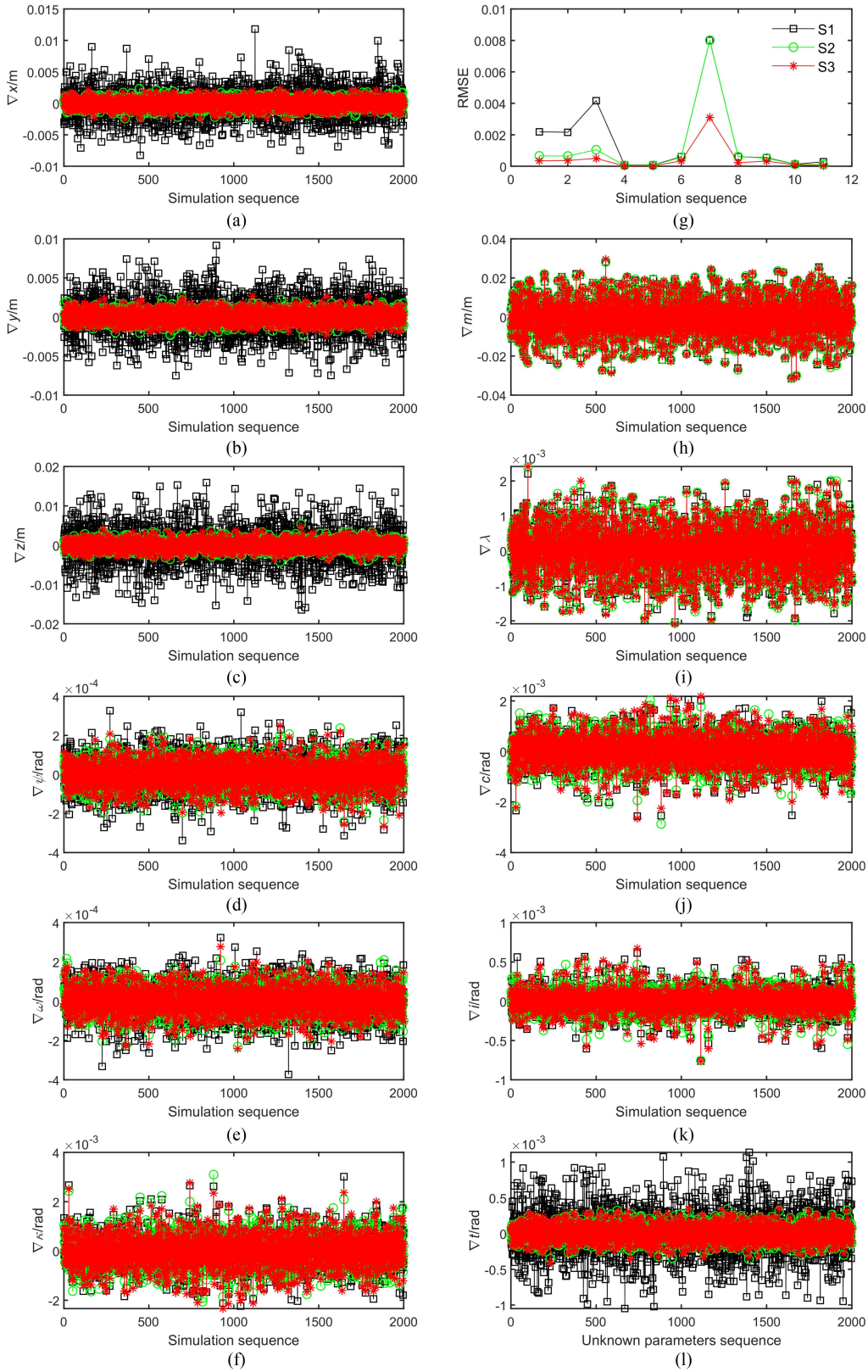

Fig. 11. Deviations of the parameters and their RMSE when the number of gross errors is 3: (a)∇x; (b)∇y; (c)∇z; (d)$\nabla \varphi$; (e)$\nabla \omega$; (f)∇k; (g) RMSE of parameters; (h)∇m; (i)$\nabla \lambda$; (j)∇c; (k)∇i; and (l)∇t.

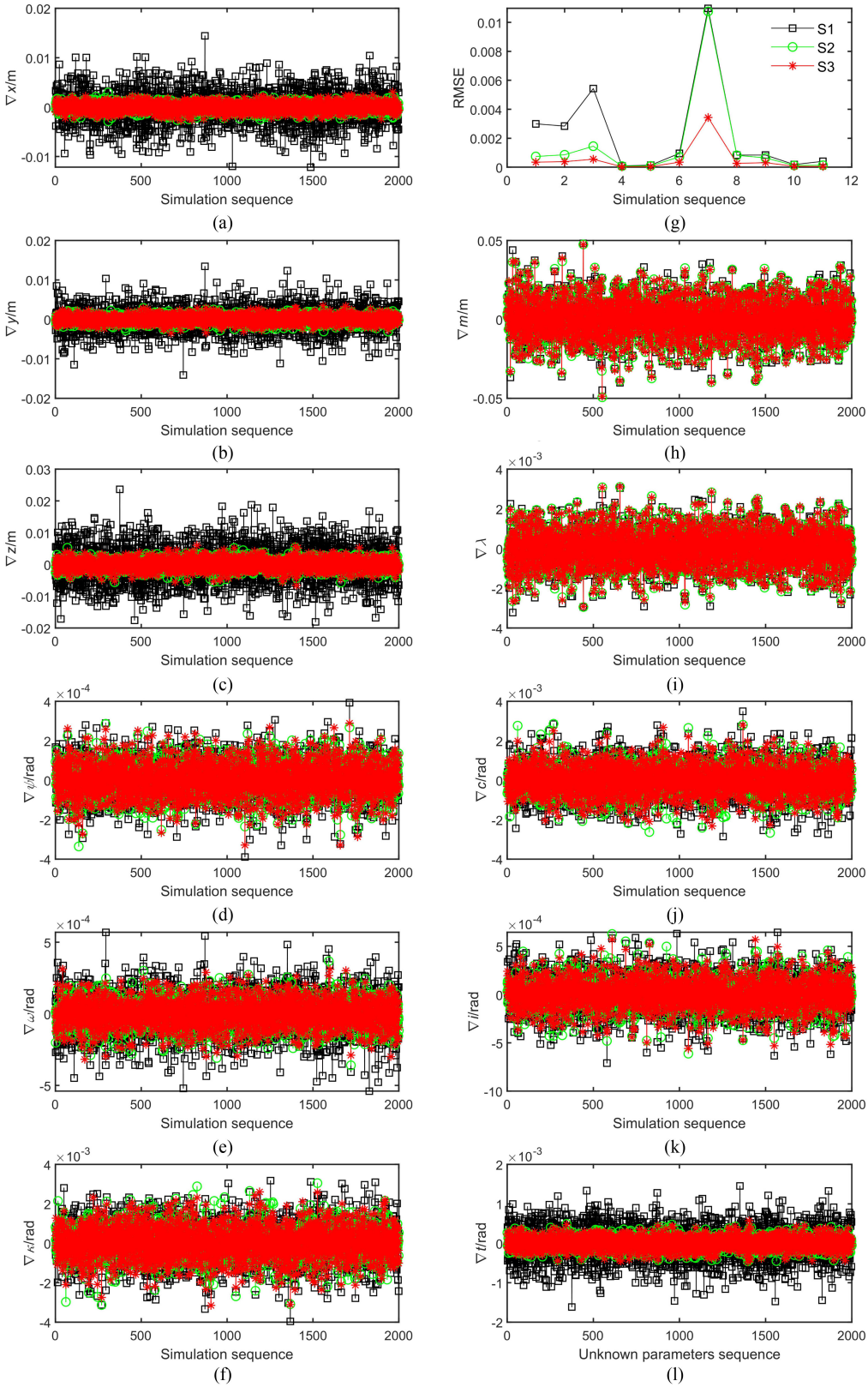

Fig. 12. Deviations of the parameters and their RMSE when the number of gross errors is 5: (a)∇x; (b)∇y; (c)∇z; (d)$\nabla \varphi$; (e)$\nabla \omega$; (f)∇k; (g) RMSE of parameters; (h)∇m; (i)$\nabla \lambda$; (j)∇c; (k)∇i; and (l)∇t.

but the robust method was indeed more valid than the nonrobust method as it could reduce the bias in the estimates to some extent after the data has been contaminated. In addition, the proposed method failed to allow for the weakening of correlations among parameters and further refinement in terms of measurement configurations would be required subsequently.

APPENDIX A

For the purpose of visualizing the deviations of the parameters and the trend of the respective RMSE of the proposed method at various NGs, the results of the calculation of 2000 simulations have been carried out compared to other three conventional methods. It ought to be clarified here that since the functional model of Scheme 1 does not incorporate CPs, so that its results are not available in (h)–(l) of Figs. 9–12. As shown in the following:

REFERENCES

[1] X. Cheng, *Theory and Techniques of Massive Point Cloud Data Processing*. Shanghai, China: Tongji Univ. Press, 2014, pp. 8–10.

[2] T. Zhou *et al.*, "A general point-based method for self-calibration of terrestrial laser scanners considering stochastic information," *Remote Sens.*, vol. 12, no. 18, 2020, Art. no. 2923.

[3] S. Kauker *et al.*, "Spatio-temporal correlations of terrestrial laser scanning," *Allgemeine Vermessungs-Nachrichten*, vol. 6, pp. 170–182, 2016.

[4] Y. Guan, X. Cheng, and X. Zhan, "Research on systematic errors calibration of terrestrial laser scanner," *Acta Geodaetica et Cartographica Sinica*, vol. 43, no. 7, pp. 731–738, 2014.

[5] T. Rabbani *et al.*, "An integrated approach for modelling and global registration of point clouds," *ISPRS J. Photogramm. Remote Sens.*, vol. 61, no. 6, pp. 355–370, Feb. 2007.

[6] D. Lichti *et al.*, "Calibration and testing of a terrestrial laser scanner," *Int. Arch. Photogramm. Remote Sens.*, vol. 33, no. B5/2; PART 5, pp. 485–492, 2000.

[7] Y. Han, L. Wang, and X. Lu, "A study of 360° laser scanner for goniometric error checking," *Eng. Surv.*, vol. 39, no. 2, pp. 59–63, 2011.

[8] J. Zhang, L. Pan, and S. Wang, *Photogrammetry*. Wuhan, China: Wuhan Univ. Press, 2003, pp. 17–20.

[9] D. D. Lichti and J. Franke, "Self-calibration of the iQsun 880 laser scanner," in *Proc. Opt.*, 2005, pp. 122–131.

[10] D. D. Lichti, "Error modelling, calibration and analysis of an AM-CW terrestrial laser scanner system," *ISPRS J. Photogramm. Remote Sens.*, vol. 61, no. 5, pp. 307–324, Jan. 2007.

[11] D. González-Aguilera *et al.*, "Trimble GX200 and riegl LMS-Z390i sensor self-calibration," *Opt. Exp.*, vol. 19, no. 3, pp. 2676–2693, 2011.

[12] C. Holst and H. Kuhlmann, "Aiming at self-calibration of terrestrial laser scanners using only one single object and one single scan," *J. Appl. Geodesy*, vol. 8, no. 4, pp. 295–310, 2014.

[13] J. L. Lerma and D. García, "Self-calibration of terrestrial laser scanners: Selection of the best geometric additional parameters," *ISPRS Ann. Photogramm. Remote Sens. Spatial Inf. Sci.*, vol. II-5, pp. 219–226, 2014.

[14] Y. Reshetyuk, "Calibration of terrestrial laser scanners callidus 1.1, leica HDS 3000 and leica HDS 2500," *Surv. Rev.*, vol. 38, no. 302, pp. 703–713, 2006.

[15] Y. Reshetyuk, "Self-calibration and direct georeferencing in terrestrial laser scanning," Ph.D. dissertation, Dept. Trans. Eco., KTH. Univ., STO, Sweden, 2009.

[16] Y. Reshetyuk, "Investigation and calibration of pulsed time-of-flight terrestrial laser scanners," M.S. dissertation, Dept. Trans. Eco., KTH. Univ., STO, Sweden, 2006.

[17] X. Li, Y. Li, X. Xie, and L. Xu, "Terrestrial laser scanner autonomous self-calibration with no prior knowledge of point-clouds," *IEEE Sensors J.*, vol. 18, no. 22, pp. 9277–9285, Nov. 2018.

[18] T. Medić, H. Kuhlmann, and C. Holst, *A Priori vs. In-Situ Terrestrial Laser Scanner Calibration in the Context of the Instability of Calibration Parameters*. Berlin, Germany: Springer, 2020.

[19] X. Li *et al.*, "Lab-built terrestrial laser scanner self-calibration using mounting angle error correction," *Opt Exp.*, vol. 26, no. 11, pp. 14444–14460, May 2018.

[20] D. D. Lichti, "Terrestrial laser scanner self-calibration: Correlation sources and their mitigation," *ISPRS J. Photogramm. Remote Sens.*, vol. 65, no. 1, pp. 93–102, Jan. 2010.

[21] Y. Reshetyuk, "A unified approach to self-calibration of terrestrial laser scanners," *ISPRS J. Photogramm. Remote Sens.*, vol. 65, no. 5, pp. 445–456, Sep. 2010.

[22] D. D. Lichti, J. Chow, and H. Lahamy, "Parameter de-correlation and model-identification in hybrid-style terrestrial laser scanner self-calibration," *ISPRS J. Photogramm. Remote Sens.*, vol. 66, no. 3, pp. 317–326, May 2011.

[23] J.-A. Paffenholz and K.-H. Bae, "Geo-referencing point clouds with transformational and positional uncertainties," *J. Appl. Geodesy*, vol. 6, 2012, Art. no. 1.

[24] D. Wujanz *et al.*, "An intensity-based stochastic model for terrestrial laser scanners," *ISPRS J. Photogramm. Remote Sens.*, vol. 125, pp. 146–155, Mar. 2017.

[25] T. Medić *et al.*, "Empirical stochastic model of detected target centroids: Influence on registration and calibration of terrestrial laser scanners," *J. Appl. Geodesy*, vol. 13, no. 3, pp. 179–197, 2019.

[26] M. A. Abbas *et al.*, "An on-site approach for the self-calibration of terrestrial laser scanner," *Measurement*, vol. 52, pp. 111–123, Jun. 2014.

[27] T. O. Chan, D. D. Lichti, and D. Belton, "A rigorous cylinder-based self-calibration approach for terrestrial laser scanners," *ISPRS J. Photogramm. Remote Sens.*, vol. 99, pp. 84–99, Jan. 2015.

[28] X. Ge, "Configuration requirements for panoramic terrestrial laser scanner calibration within a point field," *IEEE Geosci. Remote Sens. Lett.*, vol. 17, no. 11, pp. 1889–1893, Nov. 2020.

[29] A. Rietdorf, F. Gielsdorf, and L. Gruendig, "A concept for the calibration of terrestrial laser scanners," in *Proc. FIG Regional Central Eastern Eur. Conf. Eng. Surveying*, 2004, Art. no. 13.

[30] K.-H. Bae and D. Lichti, "On-site self-calibration using planar features for terrestrial laser scanners," *Int. Arch. Photogramm. Remote Sens. Spatial Inf. Sci.*, vol. 36, pp. 14–19, 2007.

[31] J. C. K. Chow, D. D. Lichti, and C. Glennie, "Point-based versus plane-based self-calibration of static terrestrial laser scanners," *ISPRS Workshop Laser Scanning*, vol. 38-5, no. W12, pp. 121–126, 2011.

[32] G. S. Cheok, S. Leigh, and A. Rukhin, "Calibration experiments of a laser scanner," *STIN*, vol. 2, 2002, Art. no. 88658.

[33] T. Schulz, *Calibration of a Terrestrial Laser Scanner for Engineering Geodesy*. Zürich, Switzerland: ETH, 2008.

[34] P. J. Teunissen and A. Amiri-Simkooei, "Least-squares variance component estimation," *J. Geodesy*, vol. 82, no. 2, pp. 65–82, 2008.

[35] S. R. Searle, "An overview of variance component estimation," *Metrika*, vol. 42, no. 1, pp. 215–230, 1995.

[36] D. Rasch and O. Masata, "Methods of variance component estimation," *Czech J. Animal Sci.*, vol. 51, no. 6, 2006, Art. no. 227.

[37] D. Schneider, "Calibration of a riegl LMS-Z420i based on a multi-station adjustment and a geometric model with additional parameters," *Int. Arch. Photogramm. Remote Sens. Spatial Inf.*, vol. 38, pp. 177–182, 2009.

[38] S. Kauker and V. Schwieger, "First investigations for a synthetic covariance matrix for monitoring by terrestrial laser scanning," in *Proc. 3rd Joint Int. Symp. Deformation Monit.*, 2016, pp. 1–10.

[39] S. Kauker and V. Schwieger, "A synthetic covariance matrix for monitoring by terrestrial laser scanning," *J. Appl. Geodesy*, vol. 11, 2017, Art. no. 2.

[40] B. Wang *et al.*, "Generalized total least squares prediction algorithm for universal 3D similarity transformation," *Adv. Space Res.*, vol. 59, no. 3, pp. 815–823, Feb. 2017.

[41] Y. Shen, B. Li, and Y. Chen, "An iterative solution of weighted total least-squares adjustment," *J. Geodesy*, vol. 85, no. 4, pp. 229–238, 2011.

[42] Y. Z. Shen, Y. Chen, and D. H. Zheng, "A quaternion-based geodetic datum transformation algorithm," *J. Geodesy*, vol. 80, no. 5, pp. 233–239, Aug. 2006.

[43] Y. Yang, L. Song, and T. J. J. O. G. Xu, "Robust estimator for correlated observations based on bifactor equivalent weights," *J. Geodesy*, vol. 76, no. 6/7, pp. 353–358, 2002.

[44] M. A. Fischler and R. C. Bolles, "Random sample consensus: A paradigm for model fitting with applications to image analysis and automated cartography," *Commun. ACM*, vol. 24, no. 6, pp. 381–395, 1981.

[45] Y. Yang, L. Song, and T. Xu, "Robust parameter estimation for geodetic correlated observations," *Acta Geodaeticaet Cartographica Sinica*, vol. 31, no. 2, pp. 95–99, 2002.

[46] B. Wang *et al.*, "Newton–Gauss algorithm of robust weighted total least squares model," *Acta Geodaeticaet Cartographica Sinica*, vol. 44, no. 6, pp. 602–608, 2015.
[47] C. Liu *et al.*, "Three-dimensional coordinate transformation model and its robust estimation method under Gauss–Helmert model," *Geomatics Inf. Sci. Wuhan Univ.*, vol. 43, no. 9, pp. 1320–1327, 2018.
[48] X. Yu and W. Lv, "Robust estimation model for correlated observations based on standardized residuals," *Geomatics Inf. Sci. Wuhan Univ.*, vol. 24, no. 1, pp. 75–78, 1999.
[49] X. Gao and W. Dai, "Application of robust Helmert variance component estimation to position in combination of GPS and BDS," *J. Geodesy Geodyn.*, vol. 34, no. 1, pp. 173–176, 2014.
[50] L. Wang, H. Chen, and Y. Lin, "Spherical target positioning of 3D laser scanning by using robust WTLS method," *J. Geodesy Geodyn.*, vol. 36, no. 8, pp. 745–749, 2016.
[51] Z. Yu, "The general formulas of Helmert type for estimating variance and covarince components," *Geomatics Inf. Sci. Wuhan Univ.*, vol. 16, no. 02, pp. 8–17, 1991.
[52] S. Zhang *et al.*, "Ground-based GPS tomography spatial water vapor distribution with robust variance components estimation," *Geomatics Inf. Sci. Wuhan Univ.*, vol. 38, no. 2, pp. 144–147, 2013.

Peng Lin received the B.S. and M.S. degrees in surveying and geo-information from Anhui University of Science and Technology, Huainan, China, in 2013 and 2015, respectively, and the Ph.D. degree in geodesy and survey engineering from China University of Mining and Technology, Xuzhou, China, in 2018.

He is currently a Lecturer with the College of Civil Engineering, Anhui Jianzhu University, Hefei, China. His research interests including point cloud data processing and three-dimensional deformation monitoring.

Xiaojun Cheng was born in Jingdezhen, China, in 1964. He received the B.S. degree in engineering surveying from Tongji University, Shanghai, China, in 1985, and the M.S. and Ph.D. degrees in geodesy from Tongji University, in 1992 and 2002, respectively.

Since 1985, he has been teaching with the College of Surveying and Geo-informatics, Tongji University, where he has also been a Professor, since 2002, and was appointed as a Ph.D. Supervisor the following year. He has authored/coauthored more than 200 articles and edited/coedited 16 textbooks. His research interests include 3-D laser scanning technology, 3-D digital simulation, and precision engineering measurement.

Prof. Cheng chaired more than 40 projects of the National Natural Science Foundation of China, supervised more than 70 master's and Ph.D. students, and was the recipient of one first-class, three second-class and two third-class provincial and ministerial teaching achievement awards, and two second-class provincial and ministerial science and technology progress awards.

Tengfei Zhou was born in Suzhou, China, in 1993. He received the B.S. and M.S. degrees in surveying and geo-information from the Anhui University of Technology, Huainan, China, in 2014 and 2017, respectively. He is currently working toward the Ph.D. degree in surveying and mapping science and technology at Tongji University, Shanghai, China.

His research interests include least squares theory, 3-D laser scanning point cloud data processing, theoretical method improvement of instrument calibration, and 3-D model construction and application.

Chao Liu was born in Pucheng, Shaanxi, China, in 1985. He received the B.S. degree in engineering surveying from China University of Mining and Technology (CUMT), Xuzhou, China, in 2007, and the Ph.D. degree in geodesy from CUMT, in 2011.

He is currently an Associate Professor with the School of Mining and Geomatics, Hebei University of Engineering, Handan, China. He has authored/coauthored more than 80 articles and edited/coedited three textbooks. His research interests include deformation monitoring, GNSS signal processing, and mine survey.

Dr. Liu has chaired over more than ten scientific research projects, including the National Natural Science Foundation of China, and has supervised more than 30 graduate students.

Bin Wang received the M.S. degree in geodesy and surveying engineering from the China University of Mining and Technology, Xuzhou, China, in 2013, and the Ph.D. degree in geodesy and surveying engineering from the School of Geodesy and Geomatics, Wuhan University, Wuhan, China, in 2017.

He is currently a Lecturer with the School of Geomatics Science and Technology, Nanjing Tech University, Nanjing, China. From 2015 to 2016, he was an Exchange Visitor supported by DAAD Thematic Network Project with the Institute of Geodesy, University of Stuttgart, Stuttgart, Germany. His research interests include generalized total least-squares algorithms and their applications in geoscience field.